

SUPPORT POINTS

BY SIMON MAK AND V. ROSHAN JOSEPH

Georgia Institute of Technology

Abstract This paper introduces a new way to compact a continuous probability distribution F into a set of representative points called *support points*. These points are obtained by minimizing the distance-based energy statistic, which was initially proposed by Székely and Rizzo (2004) for goodness-of-fit testing, but also has a rich optimization structure. Theoretically, support points can be shown to be consistent for integration use, and enjoy an improved error convergence rate to Monte Carlo methods. In practice, simulation studies show that support points provide sizable improvements for integration to *both* Monte Carlo and state-of-the-art quasi-Monte Carlo methods for moderate point set sizes n and dimensions p . Two algorithms are proposed for computing support points, both of which exploit blockwise coordinate optimization and/or resampling to generate high-quality point sets with computation time linear in n and p . Two important applications for support points are then highlighted: (a) as a way to optimally allocate runs for stochastic simulations, and (b) as an improved alternative to Markov-Chain Monte Carlo (MCMC) thinning for Bayesian computation.

1. Introduction. This paper explores a new method for compacting a continuous probability distribution F into a set of representative points (rep-points) for F , which we call *support points*. Rep-points have many important applications in both statistics and engineering, since these points can provide an improved representation of F compared to a random sample. One application is in stochastic simulation, where the use of rep-points as simulation inputs allows engineers to study how uncertainty in input variables propagate to system output. Another application is for Bayesian computation, specifically as a data-reduction technique for optimally compacting large posterior sample chains from Markov-Chain Monte Carlo (MCMC) methods [24]. In this paper, we demonstrate the excellent performance of support points for these applications, and illustrate its effectiveness for the general problem of numerical integration.

Before discussing support points, we first outline two classes of existing methods for rep-points, and describe some of their problems in practice.

62E17

Keywords and phrases: Bayesian computation, energy distance, Monte Carlo, numerical integration, Quasi Monte Carlo, representative points.

The first class involves the so-called *mse-rep-points* (see, e.g., Section 4 of [19]), which minimizes the expected (Euclidean) distance of a random point $\mathbf{Y} \sim F$ to its closest rep-point. Also known as principal points [20], mse-rep-points have been applied in a variety of statistical and engineering contexts, including quantizer design [25, 47] and optimal stratified sampling [10, 9]. In practice, these rep-points can be efficiently generated by performing k-means clustering [35] on a large sample from F and taking converged cluster centers. One weakness of these point sets, however, is that they do not necessarily converge to F (see, e.g., [56]). The second class of rep-points, called *energy rep-points*, aims to find an optimal point set which minimizes some potential on the probability space ([14] provides a good overview on potential theory). Included here are the minimum-energy designs in [28] and the minimum Riesz energy points in [3]. Although it can be shown that these point sets converge to F (see, e.g., [62]), its rate of convergence is slow both theoretically and in practice [3]. Moreover, the construction of energy rep-points can be computationally expensive in higher dimensions.

The key idea behind support points is that it *optimizes* a specific *goodness-of-fit* (GOF) statistic called the *energy distance*. First introduced in [57], this statistic was proposed as a computationally efficient alternative to the classical Kolmogorov-Smirnov (K-S) GOF statistic [30], since the latter is difficult to evaluate in high-dimensions. In addition to being *easy-to-evaluate*, the energy distance also has *several desirable properties for optimization*, which we exploit to generate support points. Moreover, as its name suggests, the energy criterion has a charming interpretation in terms of physical potential energy (see Section 8 of [59]), which makes support points a special type of energy rep-point. Contrary to the existing energy rep-points mentioned above, we prove that support points enjoy quicker convergence to Monte Carlo (MC) methods for integration, and demonstrate its effectiveness in practice compared to state-of-the-art integration techniques.

The strategy of *reverse-engineering* a GOF test forms the basis for state-of-the-art integration techniques called *Quasi-Monte Carlo* (QMC) methods (see [13] and [12] for a modern overview). To see this, first let g be a differentiable integrand, and let $\{\mathbf{x}_i\}_{i=1}^n$ be the point set (with empirical distribution, or e.d.f., F_n) used to approximate $\int g(\mathbf{x}) dF(\mathbf{x})$ with the sample average $\int g(\mathbf{x}) dF_n(\mathbf{x})$. For simplicity, assume for now that $F = U[0, 1]^p$ is the uniform distribution on the p -dimensional hypercube, which is the usual setting for QMC (similar results hold for non-uniform F with \mathcal{X} compact, see [4]). The Koksma-Hlawka inequality (see, e.g., [43]) provides the following upper bound for integration error I :

(1)

$$I(g; F, F_n) \equiv \left| \int g(\mathbf{x}) dF(\mathbf{x}) - \int g(\mathbf{x}) dF_n(\mathbf{x}) \right| \leq V_q(g) D_r(F, F_n), \quad 1/q + 1/r = 1,$$

where $V_q(g) \equiv \|\partial^p g / \partial \mathbf{x}\|_{L_q}$ is a semi-norm for g , and $D_r(F, F_n)$ is the so-called L_r -discrepancy:

$$(2) \quad D_r(F, F_n) = \left(\int_{\mathcal{X}} |F_n(\mathbf{x}) - F(\mathbf{x})|^r \, d\mathbf{x} \right)^{1/r}.$$

$D_r(F, F_n)$ provides a measure of how close the e.d.f. F_n is to the desired distribution F , with smaller values indicating a better representation. The link between GOF and integration is revealed by setting $r = \infty$ and recognizing that the L_∞ -discrepancy (or simply *discrepancy*) is the K-S statistic! In other words, by minimizing the GOF statistic $D_\infty(F, F_n)$, the inequality in (1) shows that the resulting point set provides good integration performance for a large class of integrands. A similar Koksma-Hlawka-like bound is established for the energy distance in Section 2.

Unfortunately, $D_r(F, F_n)$ can be both computationally difficult to evaluate and optimize for general distributions F . One exception is the L_2 -discrepancy for the special case of $F = U[0, 1]^p$, which has a closed-form expression given in [65]. This expression is, however, difficult to optimize, and cannot be generalized for non-uniform F . There has also been some work on directly minimizing the discrepancy $D_\infty(F, F_n)$, including the cdf-rep-points in [19] and the uniform designs in [17], but such methods are applicable only for very small point sets on $U[0, 1]^p$ (see, e.g., [18]). To this end, modern QMC methods typically use *number-theoretic* techniques to generate point sets which achieve an *asymptotically* quick decay rate for discrepancy. State-of-the-art QMC methods include the *randomly-shifted lattice rules* [53] using the component-by-component implementation of [44] (see also [42]), and the *randomly scrambled Sobol' sequences* due to [54] and [46]. These point sets enjoy a discrepancy convergence rate very close to the optimal rate of $\mathcal{O}(1/n)$ [12], and also enjoy relief from dimensionality for high-dimensional integration problems [32]. It should be mentioned that, while most QMC methods consider only integration on $U[0, 1]^p$, there are ways to map point sets on $U[0, 1]^p$ to non-uniform F . One such map is the inverse Rosenblatt transformation [51], which can be computed in closed-form for a small class of distributions. When the density for F is known up to a proportional constant, the Markov chain Quasi-Monte Carlo (MCQMC) approach [7, 61, 5] can also be used to generate QMC points for F .

Despite similarities in motivation, support points differ from QMC on two fronts. First, support points are computed by an explicit *optimization* of the energy statistic. The use of optimization can have both advantages and disadvantages. On one hand, support points can be seen as *optimal* sampling points of F for any desired sample size n . As we show in Section 4, these

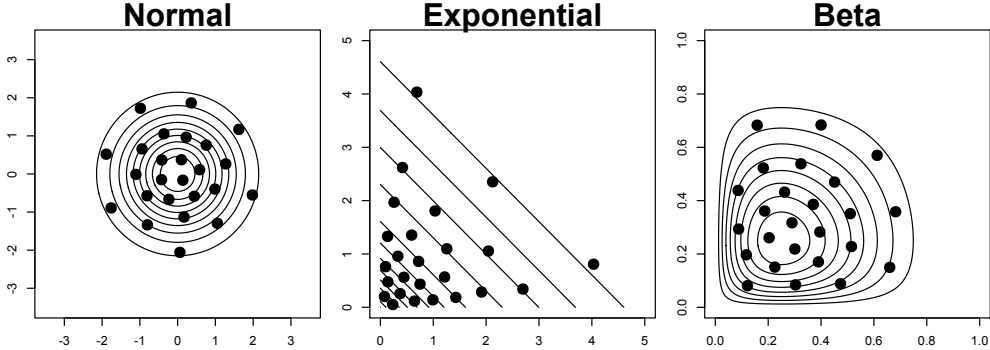


Figure 1: $n = 25$ support points for the two-dimensional $N(0, 1)$, $Exp(1)$ and $Beta(2, 4)$ distributions. Lines represent density contours.

optimized point sets can provide improved practical performance to QMC for integration. On the other hand, the computations required for optimization can grow quickly when sample size n or dimensionality p increases. To address this, two algorithms are proposed which exploit *blockwise* structure in the energy criterion to efficiently generate support points for moderate choices of $n \leq 10,000$ and $p \leq 100$. Second, since the energy statistic is *distance-based* rather than *e.d.f.-based*, support points provide better *space-fillingness* on F , meaning the point set is sufficiently spread out to maximize the representativeness of each point. Figure 1 illustrates this using $n = 25$ support points for three distributions. This contrast with, say, the MCQMC method in [5], which may return repeated samples of the same point due to Metropolis sampling, and therefore may not be optimally representative. Space-fillingness can also provide a better visual depiction of F and more robust integration performance, as we show in Section 4.

This paper is organized as follows. Section 2 first introduces support points, then provides several theorems which justifies its use for integration. Section 3 proposes two algorithms for computing support points in practice. Section 4 first outlines several simulations comparing integration performance of support points with MC and QMC methods, then provides two important applications in stochastic simulation and Bayesian computation. Section 5 concludes with some interesting directions for future research.

2. Support points. In this section, we present the theoretical basis for using support points in integration. This is presented in three parts. First, support points are defined using the energy distance in [59]. Next, the distribution convergence for support points is established, and a *Koksma-Hlawka-like* bound and an *existence* theorem are proven. The latter two

connect integration error with the energy distance, and provide an upper error bound for support points, respectively. Finally, a comparison is made between support points and MC/QMC methods, and a tighter rate is conjectured.

2.1. Definition. To begin, let us define the energy distance between two distributions F and G :

DEFINITION 1. (Def. 1 in [59]) *Let F and G be two continuous distribution functions (d.f.s) on $\mathcal{X} \subseteq \mathbb{R}^p$ with finite means, and let $\mathbf{X}, \mathbf{X}' \stackrel{i.i.d.}{\sim} G$ and $\mathbf{Y}, \mathbf{Y}' \stackrel{i.i.d.}{\sim} F$. The energy distance between F and G is defined as:*

$$(3) \quad E(F, G) \equiv 2\mathbb{E}\|\mathbf{X} - \mathbf{Y}\|_2 - \mathbb{E}\|\mathbf{X} - \mathbf{X}'\|_2 - \mathbb{E}\|\mathbf{Y} - \mathbf{Y}'\|_2.$$

When $G = F_n$ is the e.d.f. for $\{\mathbf{x}_i\}_{i=1}^n \subseteq \mathcal{X}$, this energy distance becomes:

$$(4) \quad E(F, F_n) = \frac{2}{n} \sum_{i=1}^n \mathbb{E}\|\mathbf{x}_i - \mathbf{Y}\|_2 - \frac{1}{n^2} \sum_{i=1}^n \sum_{j=1}^n \|\mathbf{x}_i - \mathbf{x}_j\|_2 - \mathbb{E}\|\mathbf{Y} - \mathbf{Y}'\|_2.$$

As mentioned earlier, the energy distance $E(F, F_n)$ was proposed as an efficient alternative to the K-S statistic in high-dimensions. Similar to the cdf-rep-points in [19], we define support points as the minimizer of $E(F, F_n)$:

DEFINITION 2. *Let $\mathbf{Y} \sim F$, where F is as defined previously. For a fixed point set size $n \in \mathbb{N}_+$, the support points of F are defined as:*

(O)

$$\{\xi_i\}_{i=1}^n \equiv \underset{\mathbf{x}_1, \dots, \mathbf{x}_n}{\operatorname{argmin}} E(F, F_n) = \underset{\mathbf{x}_1, \dots, \mathbf{x}_n}{\operatorname{argmin}} \frac{2}{n} \sum_{i=1}^n \mathbb{E}\|\mathbf{x}_i - \mathbf{Y}\|_2 - \frac{1}{n^2} \sum_{i=1}^n \sum_{j=1}^n \|\mathbf{x}_i - \mathbf{x}_j\|_2.$$

The minimization of $E(F, F_n)$ is justified by the following *metric property*:

THEOREM 1. (Prop. 2 in [59]) *Let F and G be as defined previously. Then $E(F, G) = 0$ if and only if $F \stackrel{a.s.}{=} G$, otherwise $E(F, G) > 0$.*

In words, this theorem shows that the energy between two distributions equals zero if and only if these distributions are equal almost surely. $E(F, G)$ can then be viewed as a metric on the space of distribution functions, with *smaller* values suggesting F and G are more *similar*. In this sense, support points aim to recover *optimal* sampling points which *best represent* F .

It is worth noting that the appeal of $E(F, F_n)$ as an optimization objective is akin to its original appeal for GOF testing. As mentioned earlier, $E(F, F_n)$ was proposed as an easy-to-evaluate alternative to the classical GOF tests.

However, not only is $E(F, F_n)$ *easy-to-evaluate*, it has desirable properties which make it *amenable for optimization!* In Section 3, we propose an algorithm which exploits this structure to efficiently generate support points.

For the univariate case of $p = 1$, an interesting equivalence can be established between support points and optimal L_2 -discrepancy points:

PROPOSITION 1. *Let F be a univariate distribution with finite mean. Then the support points of F are equal to the minimal L_2 -discrepancy points.*

PROOF. It can be shown [59] that $E(F, F_n) = 2D_2^2(F, F_n)$, where F_n be the e.d.f. of $\{x_i\}_{i=1}^n \subseteq \mathcal{X}$ and $D_2(F, F_n)$ is the one-dimensional L_2 -discrepancy in (2). This proves the assertion. \square

Unfortunately, this equivalence fails to hold for $p > 1$, since D_2 is not rotation-invariant. Hence, support points and optimal L_2 -discrepancy points can behave quite differently in the multivariate setting.

2.2. Theoretical properties. Although the idea of *reverse engineering* the energy GOF test is intuitively appealing, it is not clear yet why support points are *appropriate* for integration. To this end, we provide three theorems below which justify this application. The first theorem proves the convergence of support points to the desired distribution F , the second establishes a Koksma-Hlawka-like bound connecting integration error with $E(F, F_n)$, and the last provides an existence result for the convergence rate of this error.

THEOREM 2. *Let $\mathbf{X} \sim F$ and $\mathbf{X}_n \sim F_n$, where F is as defined before, and F_n is the e.d.f. of the support points in (O). Then $\mathbf{X}_n \xrightarrow{d} \mathbf{X}$.*

This relies on the following lemma, which slightly extends the Lévy continuity theorem to the *almost-everywhere (a.e.) pointwise convergence* setting.

LEMMA 1. *Let $\{F_n\}_{n=1}^\infty$ be a sequence of d.f.s with characteristic functions (c.f.s) $\{\phi_n(\mathbf{t})\}_{n=1}^\infty$, and let F be a d.f. with c.f. $\phi(\mathbf{t})$. If $\mathbf{X}_n \sim F_n$ and $\mathbf{X} \sim F$, with $\lim_{n \rightarrow \infty} \phi_n(\mathbf{t}) = \phi(\mathbf{t})$ a.e. (in the Lebesgue sense), then $\mathbf{X}_n \xrightarrow{d} \mathbf{X}$.*

PROOF. See supplementary materials. \square

PROOF. (Theorem 2) Let $\{\mathbf{Y}_i\}_{i=1}^\infty \xrightarrow{i.i.d.} F$, and let \tilde{F}_n denote the e.d.f. of $\{\mathbf{Y}_i\}_{i=1}^n$. By the Glivenko-Cantelli lemma, $\lim_{n \rightarrow \infty} \sup_{\mathbf{x} \in \mathbb{R}^p} |\tilde{F}_n(\mathbf{x}) - F(\mathbf{x})| = 0$, so $\tilde{F}_n \xrightarrow{d} F$. Let $\phi(\mathbf{t})$ and $\tilde{\phi}_n(\mathbf{t})$ denote the c.f.s of F and \tilde{F}_n , respectively.

Since $|\exp\{i\langle \mathbf{t}, \mathbf{x} \rangle\}| \leq 1$ is bounded, the Portmanteau theorem (Theorem 8.4.1 in [50]) gives:

$$(5) \quad \lim_{n \rightarrow \infty} \mathbb{E}[|\phi(\mathbf{t}) - \tilde{\phi}_n(\mathbf{t})|^2] = 0.$$

By Proposition 1 in [59], the expected energy between \tilde{F}_n and F is:

$$(6) \quad \mathbb{E}[E(F, \tilde{F}_n)] = \frac{1}{a_p} \mathbb{E} \left[\int \frac{|\phi(\mathbf{t}) - \tilde{\phi}_n(\mathbf{t})|^2}{\|\mathbf{t}\|_2^{p+1}} d\mathbf{t} \right] = \frac{1}{a_p} \int \frac{\mathbb{E} [|\phi(\mathbf{t}) - \tilde{\phi}_n(\mathbf{t})|^2]}{\|\mathbf{t}\|_2^{p+1}} d\mathbf{t},$$

where a_p is some constant depending on p , with the last step following from Fubini's theorem. It follows that $\mathbb{E} [|\phi(\mathbf{t}) - \tilde{\phi}_n(\mathbf{t})|^2] = \frac{1}{n} \text{Var} [\exp\{i\langle \mathbf{t}, \mathbf{Y}_1 \rangle\}]$, so $\mathbb{E} [|\phi(\mathbf{t}) - \tilde{\phi}_n(\mathbf{t})|^2]$ is monotonically decreasing in n . By monotone convergence and (5), we have:

$$(7) \quad \lim_{n \rightarrow \infty} \mathbb{E}[E(F, \tilde{F}_n)] = \frac{1}{a_p} \int \lim_{n \rightarrow \infty} \frac{\mathbb{E}[|\phi(\mathbf{t}) - \tilde{\phi}_n(\mathbf{t})|^2]}{\|\mathbf{t}\|_2^{p+1}} d\mathbf{t} = 0.$$

Consider now the e.d.f. of support points, F_n and its c.f. ϕ_n . By Definition 2, $E(F, F_n) \leq \mathbb{E}[E(F, \tilde{F}_n)]$, so $\lim_{n \rightarrow \infty} E(F, F_n) = 0$ by (7). Using Fatou's lemma on (6), we get:

$$\begin{aligned} 0 = \liminf_{n \rightarrow \infty} E(F, F_n) &\leq \int \liminf_{n \rightarrow \infty} \frac{|\phi(\mathbf{t}) - \phi_n(\mathbf{t})|^2}{\|\mathbf{t}\|_2^{p+1}} d\mathbf{t} \\ &\leq \int \limsup_{n \rightarrow \infty} \frac{|\phi(\mathbf{t}) - \phi_n(\mathbf{t})|^2}{\|\mathbf{t}\|_2^{p+1}} d\mathbf{t} \leq \limsup_{n \rightarrow \infty} E(F, F_n) = 0, \end{aligned}$$

which gives $\lim_{n \rightarrow \infty} |\phi(\mathbf{t}) - \phi_n(\mathbf{t})|^2 = 0$ a.e. Hence, $\phi_n(\mathbf{t}) \rightarrow \phi(\mathbf{t})$ a.e., and by Lemma 1, $\mathbf{X}_n \xrightarrow{d} \mathbf{X}$, as desired. \square

In words, this theorem shows that support points are indeed *representative* of the desired distribution F when the number of points n grow large. This allows us to establish the *consistency* of support points below.

COROLLARY 1. *Let $\mathbf{X} \sim F$ and $\mathbf{X}_n \sim F_n$, where F and F_n are as defined in Theorem 2. For any continuous map $g : \mathcal{X} \rightarrow \mathbb{R}$: (a) $g(\mathbf{X}_n) \xrightarrow{d} g(\mathbf{X})$, (b) If \mathcal{X} is compact, then $\lim_{n \rightarrow \infty} \mathbb{E}[g(\mathbf{X}_n)] = \lim_{n \rightarrow \infty} \frac{1}{n} \sum_{i=1}^n g(\xi_i) = \mathbb{E}[g(\mathbf{X})]$.*

PROOF. (a) follows from the continuous mapping theorem and Theorem 2. (b) follows by the boundedness of g on \mathcal{X} and the Portmanteau theorem. \square

The purpose of this corollary is two-fold: it not only establishes the *consistency* of support points for integration use, but also provides the justification for employing these point sets in a variety of other applications. Specifically, part (a) shows that support points are appropriate for performing *uncertainty propagation* in stochastic simulations, a point which we demonstrate in Section 4.2. Part (b) shows that, when the sample space \mathcal{X} is compact, any continuous integrand g can be *consistently estimated* using support points, i.e., its n -point integration rule converge to the desired integrand. In practice, this compactness assumption is not too restrictive, since a truncation can always be performed on \mathcal{X} to capture probability mass arbitrarily close to 1.

It is still unclear why the energy distance is a *good* criterion for integration. The next theorem justifies this by showing the squared integration error $I^2(g; F, F_n)$ in (1) can be bounded above by a term proportional to $E(F, F_n)$:

THEOREM 3. *Let F be as defined before, with $\mathcal{X} \subseteq \mathbb{R}^p$ compact. For any polynomial integrand $g : \mathcal{X} \rightarrow \mathbb{R}$:*

$$(8) \quad I(g; F, F_n) \leq \sqrt{V(g)E(F, F_n)},$$

where $I(g; F, F_n)$ is defined in (1) and $V(g)$ is a constant depending on g .

The proof of this theorem relies on the following definition and lemma.

DEFINITION 3. *For $\mathcal{X} \subseteq \mathbb{R}^p$, a function $h : \mathcal{X} \times \mathcal{X} \rightarrow \mathbb{R}$ is conditionally and integrally positive definite (c.p.d.) iff, for any function $c : \mathcal{X} \rightarrow \mathbb{R}$ satisfying $\int_{\mathcal{X}} c(\mathbf{x}) d\mathbf{x} = 0$, $\int_{\mathcal{X}} \int_{\mathcal{X}} h(\mathbf{x}, \mathbf{y}) c(\mathbf{x}) c(\mathbf{y}) d\mathbf{x} d\mathbf{y} \geq 0$. Moreover, h is strictly c.p.d. when this inequality holds strictly for all $c(\mathbf{x}) \neq 0$.*

LEMMA 2. *Let $\mathcal{X} \subseteq \mathbb{R}^p$ be compact, and let $\{\phi_k(\mathbf{x})\}_{k=0}^{\infty}$ be an orthonormal basis for $\mathcal{L}_2(\mathcal{X})$ with $\phi_0(\mathbf{x}) = 1$. For any symmetric c.p.d. function $h \in \mathcal{L}_2(\mathcal{X} \times \mathcal{X})$, $\exists(\lambda_k)_{k=0}^{\infty}, \lambda_1, \lambda_2, \dots \geq 0$ such that $h(\mathbf{x}, \mathbf{y}) = \sum_{k=0}^{\infty} \lambda_k \phi_k(\mathbf{x}) \phi_k(\mathbf{y})$ for any $\mathbf{x}, \mathbf{y} \in \mathcal{X}$. A similar statement holds for all symmetric, strictly c.p.d. functions with the modification that $\lambda_1, \lambda_2, \dots > 0$.*

PROOF. Since $h \in \mathcal{L}_2(\mathcal{X} \times \mathcal{X})$ and $\{\phi_k(\mathbf{x})\}_{k=0}^{\infty}$ forms an orthogonal basis on $\mathcal{L}_2(\mathcal{X})$, the asserted expansion of h must exist. Taking $\int \int \cdot \phi_k(\mathbf{x}) \phi_k(\mathbf{y}) d\mathbf{x} d\mathbf{y}$ on both sides of this expansion, we get $\lambda_k = \int \int h(\mathbf{x}, \mathbf{y}) \phi_k(\mathbf{x}) \phi_k(\mathbf{y}) d\mathbf{x} d\mathbf{y}$. Note that $\int_{\mathcal{X}} \phi_k(\mathbf{x}) d\mathbf{x} = 0$ for any $k \geq 1$, since $\phi_0(\mathbf{x}) = 1$. Using this along with Definition 3, the first part of the lemma is proven. The second part follows by a similar argument. \square

PROOF. (*Theorem 3*) First, rewrite $I^2(g; F, F_n)$ as:

$$\begin{aligned}
 (9) \quad I^2(g; F, F_n) &= \left[\int g(\mathbf{x}) d[F - F_n](\mathbf{x}) \right]^2 \\
 &= \int \int g(\mathbf{x})g(\mathbf{y}) d[F - F_n](\mathbf{x}) d[F - F_n](\mathbf{y}) \\
 &= \int \int \frac{1}{2} \{g^2(\mathbf{x}) + g^2(\mathbf{y}) - [g(\mathbf{x}) - g(\mathbf{y})]^2\} r(\mathbf{x})r(\mathbf{y}) dQ(\mathbf{x})dQ(\mathbf{y})
 \end{aligned}$$

where Q is a probability measure dominating both F and F_n , and $r(\mathbf{x})$ is the difference of Radon-Nikodym derivatives $r(\mathbf{x}) = \frac{dF(\mathbf{x})}{dQ} - \frac{dF_n(\mathbf{x})}{dQ}$. Since $\int \int g^2(\mathbf{x}) d[F - F_n](\mathbf{x}) d[F - F_n](\mathbf{y}) = 0$, the first and second terms in the last expression of (9) equal 0. Hence:

$$(10) \quad I^2(g; F, F_n) = -\frac{1}{2} \int \int [g(\mathbf{x}) - g(\mathbf{y})]^2 r(\mathbf{x})r(\mathbf{y}) dQ(\mathbf{x}) dQ(\mathbf{y}).$$

Consider both $h_1(\mathbf{x}, \mathbf{y}) = -\frac{1}{2}[g(\mathbf{x}) - g(\mathbf{y})]^2$ and $h_2(\mathbf{x}, \mathbf{y}) = -\|\mathbf{x} - \mathbf{y}\|_2$. By the above argument, h_1 must be c.p.d., since $I^2 \geq 0$. Moreover, by Prop. 3 of [59], h_2 is a *strictly* c.p.d. function. Since \mathcal{X} is compact, assume without loss of generality that $\mathcal{X} = [-1, 1]^p$. Let $\phi_{\mathbf{k}}(\mathbf{x})$ be the tensor product of Legendre polynomials $\phi_{\mathbf{k}}(\mathbf{x}) = \prod_{l=1}^p L_{k_l}(x_l)$, where $L_k(x)$ is the Legendre polynomial of degree k , and \mathbf{k} is the multi-index with $|\mathbf{k}| = \sum_{l=1}^p k_l$. Since $\phi_{\mathbf{0}}(\mathbf{x}) = 1$ and $\{\phi_{\mathbf{k}}(\mathbf{x})\}_{|\mathbf{k}|=0}^{\infty}$ forms an orthonormal basis of $L_2(\mathcal{X})$, Lemma 2 gives:

$$h_1(\mathbf{x}, \mathbf{y}) = \sum_{|\mathbf{k}|=0}^{\infty} \lambda_{1,\mathbf{k}} \phi_{\mathbf{k}}(\mathbf{x}) \phi_{\mathbf{k}}(\mathbf{y}) \quad \text{and} \quad h_2(\mathbf{x}, \mathbf{y}) = \sum_{|\mathbf{k}|=0}^{\infty} \lambda_{2,\mathbf{k}} \phi_{\mathbf{k}}(\mathbf{x}) \phi_{\mathbf{k}}(\mathbf{y}).$$

where $\lambda_{1,\mathbf{k}} \geq 0$ and $\lambda_{2,\mathbf{k}} > 0$ for all $|\mathbf{k}| \geq 1$.

Since g is a polynomial, say of degree q , h_1 must be a polynomial of at most degree $2q$. This means $\lambda_{1,\mathbf{k}} = 0$ for $|\mathbf{k}| > 2q$, i.e., the series for h_1 terminates *finitely*. Letting $V(g) = \max_{1 \leq |\mathbf{k}| \leq 2q} \frac{\lambda_{1,\mathbf{k}}}{\lambda_{2,\mathbf{k}}}$, it follows that $\lambda_{1,\mathbf{k}} \leq V(g)\lambda_{2,\mathbf{k}}$ for all $1 \leq |\mathbf{k}| \leq 2q$. Combining this with $\int r(\mathbf{x}) dQ(\mathbf{x}) = 0$, (10) becomes:

$$\begin{aligned}
 I^2(g; F, F_n) &= \int \int \left\{ \sum_{|\mathbf{k}|=0}^{\infty} \lambda_{1,\mathbf{k}} \phi_{\mathbf{k}}(\mathbf{x}) \phi_{\mathbf{k}}(\mathbf{y}) \right\} r(\mathbf{x})r(\mathbf{y}) dQ(\mathbf{x}) dQ(\mathbf{y}) \\
 &= \sum_{|\mathbf{k}|=1}^{2q} \lambda_{1,\mathbf{k}} \left\{ \int \phi_{\mathbf{k}}(\mathbf{x})r(\mathbf{x}) dQ(\mathbf{x}) \right\}^2 \\
 &\leq V(g) \sum_{|\mathbf{k}|=1}^{2q} \lambda_{2,\mathbf{k}} \left\{ \int \phi_{\mathbf{k}}(\mathbf{x})r(\mathbf{x}) dQ(\mathbf{x}) \right\}^2
 \end{aligned}$$

$$\begin{aligned}
&\leq V(g) \int \int \left\{ \sum_{|\mathbf{k}|=0}^{\infty} \lambda_{2,\mathbf{k}} \phi_{\mathbf{k}}(\mathbf{x}) \phi_{\mathbf{k}}(\mathbf{y}) \right\} r(\mathbf{x}) r(\mathbf{y}) dQ(\mathbf{x}) dQ(\mathbf{y}) \\
&= -V(g) \int \int \|\mathbf{x} - \mathbf{y}\|_2 r(\mathbf{x}) r(\mathbf{y}) dQ(\mathbf{x}) dQ(\mathbf{y}) = V(g) E(F, F_n),
\end{aligned}$$

where the last step follows from Theorem 1 in [58]. \square

This theorem provides a Koksma-Hlawka-like bound by connecting the error $I(g; F, F_n)$ with the energy distance $E(F, F_n)$. Similar to the use of the Koksma-Hlawka inequality for QMC, Theorem 3 justifies the application of support points for integration by showing the integration error for all polynomials can be sufficiently bounded by minimizing $E(F, F_n)$. Although this is shown only for polynomials, simulation studies in Section 4 show that support points are also adept at integrating non-polynomial integrands. Demonstrating this theoretically is therefore a direction for future work.

A natural point to investigate next is the convergence of $I(g; F, F_n)$ under support points. The theorem below provides an *existence* result which demonstrates the existence of a point set sequence achieving the energy decay rate in (11). Using Theorem 3, an upper bound for $I(g; F, F_n)$ can then be obtained. We preface this by emphasizing that the *main goal* of this theorem is to show that support points enjoy a *theoretical improvement over Monte Carlo*; from the simulations in Section 4, the asserted rate appears to be far from tight. A tighter rate is conjectured in Section 2.3.

THEOREM 4. *Let F be as defined before, with $\mathcal{X} \subseteq \mathbb{R}^p$ compact, and let F_n be the e.d.f. for the set of n support points. Then, for any $0 < \nu < 1$, $\exists C_{\nu,p} > 0$ such that:*

$$(11) \quad E(F, F_n) \leq C_{\nu,p} n^{-1} (\log n)^{-(1-\nu)/p},$$

This provides an error convergence rate of:

$$(12) \quad I(g; F, F_n) \leq \sqrt{V(g) C_{\nu,p}} n^{-1/2} (\log n)^{-(1-\nu)/(2p)}.$$

The main idea in this proof exploits the fact that $E(F, F_n)$ is a goodness-of-fit statistic. Specifically, writing $E(F, F_n)$ as a *degenerate V-statistic* V_n , we appeal to its limiting distribution and a uniform Barry-Esseen-like rate to derive an upper bound for the minimum of V_n . This is detailed below.

LEMMA 3. [26] *Let h be a symmetric, positive definite (p.d.) function satisfying the degeneracy condition $\mathbb{E}[h(\mathbf{x}, \mathbf{Y})] = 0$, with $\mathbf{Y} \sim F$. Define*

the V -statistic for h as $V_n \equiv \frac{1}{n^2} \sum_{i=1}^n \sum_{j=1}^n h(\mathbf{Y}_i, \mathbf{Y}_j)$, where $\{\mathbf{Y}_i\}_{i=1}^\infty \stackrel{i.i.d.}{\sim} F$. Then $W_n \equiv nV_n \xrightarrow{d} \sum_{k=1}^\infty \lambda_k \chi_k^2 \equiv W_\infty$, where $\{\chi_k^2\}_{k=1}^\infty \stackrel{i.i.d.}{\sim} \chi^2(1)$, and $\lambda_1 \geq \lambda_2 \geq \dots > 0$, $\sum_{k=1}^\infty \lambda_k < \infty$ are the eigenvalues of h satisfying the integral equations $\lambda_k \phi_k(\mathbf{x}) = \mathbb{E}[h(\mathbf{x}, \mathbf{Y}) \phi_k(\mathbf{Y})]$, $\mathbb{E}[\phi_k^2(\mathbf{Y})] = 1$.

LEMMA 4. (pg. 82 of [31]) Let W_n and W_∞ be as defined in Lemma 3, with d.f.s F_{W_n} and F_{W_∞} . If \mathcal{X} is compact, $\exists c_p > 0$ such that:

$$(13) \quad \sup_x |F_{W_n}(x) - F_{W_\infty}(x)| \leq c_p n^{-1/2}.$$

LEMMA 5. Let F be a continuous d.f. with compact $\mathcal{X} \subseteq \mathbb{R}^p$, and let $\mathbf{Y} \sim F$. Define $h(\mathbf{x}, \mathbf{y}) = \mathbb{E}\|\mathbf{x} - \mathbf{Y}\|_2 + \mathbb{E}\|\mathbf{y} - \mathbf{Y}\|_2 - \mathbb{E}\|\mathbf{Y} - \mathbf{Y}'\|_2 - \|\mathbf{x} - \mathbf{y}\|_2$ (which is symmetric and p.d., see [67]), and let $\{\lambda_k\}_{k=1}^\infty$ be as defined in Lemma 3. Then $\exists c_p > 0$ such that $\lambda_k \leq c_p k^{-1-1/p}$.

PROOF. This follows from Theorem 4 in [8] when $h(\mathbf{x}, \mathbf{y})$ is Lipschitz, i.e., $\exists L < \infty$ such that $\sup_{\mathbf{z} \in \mathcal{X}} |h(\mathbf{x}, \mathbf{z}) - h(\mathbf{y}, \mathbf{z})| \leq L \|\mathbf{x} - \mathbf{y}\|_2$. But:

$$\begin{aligned} |h(\mathbf{x}, \mathbf{z}) - h(\mathbf{y}, \mathbf{z})| &= |\mathbb{E}\|\mathbf{x} - \mathbf{Y}\|_2 - \|\mathbf{x} - \mathbf{z}\|_2 - \mathbb{E}\|\mathbf{y} - \mathbf{Y}\|_2 + \|\mathbf{y} - \mathbf{z}\|_2| \\ &\leq \int \left| \|\mathbf{x} - \mathbf{z}\|_2 - \|\mathbf{y} - \mathbf{z}\|_2 \right| dF(\mathbf{z}) + \left| \|\mathbf{x} - \mathbf{z}\|_2 - \|\mathbf{y} - \mathbf{z}\|_2 \right| \\ &\leq \int \|\mathbf{x} - \mathbf{y}\|_2 dF(\mathbf{z}) + \|\mathbf{x} - \mathbf{y}\|_2 \leq 2\|\mathbf{x} - \mathbf{y}\|_2, \end{aligned}$$

where the last step holds by the triangle inequality, since $\|\mathbf{x} - \mathbf{z}\|_2 - \|\mathbf{y} - \mathbf{z}\|_2 \leq \|\mathbf{x} - \mathbf{y}\|_2$ and $\|\mathbf{y} - \mathbf{z}\|_2 - \|\mathbf{x} - \mathbf{z}\|_2 \leq \|\mathbf{x} - \mathbf{y}\|_2$. This completes the proof. \square

LEMMA 6. (Paley-Zygmund inequality, [48]) Let $X \geq 0$, with constants $a_1 > 1$ and $a_2 > 0$ satisfying $\mathbb{E}(X^2) \leq a_1 \mathbb{E}^2(X)$ and $\mathbb{E}(X) \geq a_2$. Then, for any $\theta \in (0, 1)$, $\mathbb{P}(X \geq a_2\theta) \geq (1 - \theta)^2/a_1$.

The proof of Theorem 4 then follows:

PROOF. (Theorem 4) Following Section 1 of [59], the energy distance $E(F, F_n)$ can be written as the order-2 V -statistic:

$$(14) \quad E(F, F_n) = \frac{1}{n^2} \sum_{i=1}^n \sum_{j=1}^n h(\boldsymbol{\xi}_i, \boldsymbol{\xi}_j) \leq \frac{1}{n^2} \sum_{i=1}^n \sum_{j=1}^n h(\mathbf{Y}_i, \mathbf{Y}_j) \equiv V_n,$$

where $h(\mathbf{x}, \mathbf{y})$ is defined in Lemma 5 and $\{\mathbf{Y}_i\}_{i=1}^n \stackrel{i.i.d.}{\sim} F$. The last inequality follows since support points minimize $E(F, F_n)$. Invoking Lemma 3, we have:

$$(15) \quad \inf\{x : F_{W_n}(x) > 0\} = nE(F, F_n),$$

The strategy is to obtain a lower bound on the left-tail of W_∞ , then use this to derive an upper bound for $\inf\{x : F_{W_n}(x) > 0\}$ using Lemma 4.

We first investigate the left-tail behavior of W_∞ . Define $Z_t = \exp\{-tW_\infty\}$ for some $t > 0$ to be determined later. Since Z_t is bounded a.s., $\mathbb{E}(Z_t) = \prod_{k=1}^{\infty} (1 + 2\lambda_k t)^{-1/2}$ and $\mathbb{E}(Z_t^2) = \prod_{k=1}^{\infty} (1 + 4\lambda_k t)^{-1/2}$. From Lemma 6, it follows that, for fixed $x > 0$, if our choice of t satisfies:

$$(16) \quad [\mathbf{A1}] : \mathbb{E}(Z_t) \geq 2 \exp\{-tx\} > \exp\{-tx\}, \quad [\mathbf{A2}] : \mathbb{E}(Z_t^2) \leq a_1 \mathbb{E}^2(Z_t),$$

then, setting $\theta = 1/2$ and $a_2 = \exp\{-tx\}$, we have:

$$(17) \quad F_{W_\infty}(x) = \mathbb{P}(Z \geq \exp\{-tx\}) \geq \mathbb{P}(Z \geq \mathbb{E}(Z)/2) \geq (4a_1)^{-1}.$$

Consider **[A1]**, or equivalently: $tx \geq \log 2 + (1/2) \sum_{k=1}^{\infty} \log(1 + 2\lambda_k t)$. Let $\alpha = 1 + (1 - \nu)/p$, and note that, by Lemma 5, $\sum_{k=1}^{\infty} \lambda_k^\alpha < \infty$. Since $\log(1 + x) \leq x^q/q$ for $x > 0$ and $0 < q < 1$, a sufficient condition for **[A1]** is:

$$tx \geq \log 2 + (\alpha/2) \sum_{k=1}^{\infty} (2\lambda_k t)^{1/\alpha} \Leftrightarrow P_\alpha(s) \equiv s^\alpha - b_{\nu,p} s x^{-1} - (\log 2) x^{-1} \geq 0,$$

where $s = t^{1/\alpha}$ and $b_{\nu,p} = \alpha 2^{1/\alpha-1} \sum_{k=1}^{\infty} \lambda_k^{1/\alpha} > 0$.

Since $\log 2 > 0$ and $b_{\nu,p} s x^{-1} > 0$, there exists exactly one (real) positive root for $P_\alpha(s)$. Call this root r , so the above inequality is satisfied for $s > r$. Define $\bar{P}_\alpha(s)$ as the linearization of $P_\alpha(s)$ for $s > \bar{s} = (b_{\nu,p} x^{-1})^{1/(\alpha-1)}$, i.e.:

$$\bar{P}_\alpha(s) = \begin{cases} P_\alpha(s), & 0 \leq s \leq \bar{s} \\ -x^{-1} \log 2 + P'_\alpha(\bar{s}) \cdot (s - \bar{s}), & s > \bar{s}. \end{cases}$$

From this, the unique root of $\bar{P}_\alpha(s)$ can be shown to be $\bar{r} = \bar{s} + x^{-1}(\log 2)[P'_\alpha(\bar{s})]^{-1}$. Since $P_\alpha(s) \geq \bar{P}_\alpha(s)$ for all $s \geq 0$, $\bar{r} \geq r$, the following upper bound for \bar{r} can be obtained for sufficiently small x :

$$\bar{r} = (b_{\nu,p} x^{-1})^{1/(\alpha-1)} + (\log 2)(\alpha - 1)^{-1} b_{\nu,p}^{-1} \leq 2(b_{\nu,p} x^{-1})^{1/(\alpha-1)}.$$

Hence:

$$(18) \quad \begin{aligned} t = s^\alpha \geq 2^\alpha (b_{\nu,p} x^{-1})^{\alpha/(\alpha-1)} &\Leftrightarrow s \geq 2(b_{\nu,p} x^{-1})^{1/(\alpha-1)} \geq \bar{r} \geq r \\ &\Rightarrow s^\alpha - b_{\nu,p} x^{-1} s - (\log 2) x^{-1} \geq 0, \end{aligned}$$

so setting $t = 2^\alpha (b_{\nu,p} x^{-1})^{\alpha/(\alpha-1)} \equiv c_{\nu,p} x^{-\alpha/(\alpha-1)}$ satisfies **[A1]** in (16).

The next step is to determine the smallest a_1 satisfying [A2] in (16), or equivalently, $\frac{1}{2} \sum_{k=1}^{\infty} \log(1+4\lambda_k t) \geq \sum_{k=1}^{\infty} \log(1+2\lambda_k t) - \log a_1$. Again, since $\log(1+x) \leq x^q/q$ for $x > 0$ and $0 < q < 1$, a sufficient condition for [A2] is:

$$\log a_1 \geq \sum_{k=1}^{\infty} \log(1+2\lambda_k t) \Leftrightarrow \log a_1 \geq \alpha \sum_{k=1}^{\infty} (2\lambda_k t)^{1/\alpha}$$

Plugging in $t = c_{\nu,p} x^{-\alpha/(\alpha-1)}$ from (18) and letting $d_{\nu,p} \equiv \alpha(2c_{\nu,p})^{1/\alpha} \left(\sum_{k=1}^{\infty} \lambda_k^{1/\alpha} \right)$, we get $\log a_1 \geq d_{\nu,p} x^{-1/(\alpha-1)} \Leftrightarrow a_1 \geq \exp \{ d_{\nu,p} x^{-1/(\alpha-1)} \}$.

The choice of $t = c_{\nu,p} x^{-\alpha/(\alpha-1)}$ and $a_1 = \exp \{ d_{\nu,p} x^{-1/(\alpha-1)} \}$ therefore [A1] and [A2] in (17). It follows from (17) that:

$$(19) \quad F_{W_{\infty}}(x) \geq (4a_1)^{-1} = \exp \{ -d_{\nu,p} x^{-1/(\alpha-1)} \} / 4,$$

so $F_{W_{\infty}}(x)$ converges to 0 at a rate of $\mathcal{O}(\exp \{ -d_{\nu,p} x^{-1/(\alpha-1)} \})$ as $x \rightarrow 0^+$.

With this in hand, we then investigate the behavior of $\inf \{x : F_{W_n}(x) > 0\}$ as $n \rightarrow \infty$. From the uniform bound in Lemma 4, there exists some constant c_p such that $|F_{W_n}(x) - F_{W_{\infty}}(x)| \leq c_p n^{-1/2}$ for any $n \in \mathbb{N}$. Setting the right side of (19) equal to $2c_p n^{-1/2}$ and solving for x , we get:

$$(20) \quad x^* = \frac{d_{\nu,p}^{\alpha-1}}{[\log \{ n^{1/2} / (8c_{\nu,p}) \}]^{\alpha-1}} \Rightarrow F_{W_{\infty}}(x^*) \geq \exp \{ -d_{\nu,p} (x^*)^{-1/(\alpha-1)} \} = 2c_p n^{-1/2}.$$

so Lemma 4 ensures the above choice of x^* satisfies $F_{W_n}(x^*) \geq c_p n^{-1/2} > 0$.

Using this with (15), it follows that $\exists C_{\nu,p} > 0$ such that:

$$nE(F, F_n) \leq x^* = C_{\nu,p} (\log n)^{-(\alpha-1)} \Leftrightarrow E(F, F_n) \leq C_{\nu,p} n^{-1} (\log n)^{-(1-\nu)/p}.$$

Finally, by the error bound in Theorem 3, we have:

$$I(g; F, \{\xi_i\}_{i=1}^n) \leq \sqrt{V(g) C_{\nu,p} n^{-1/2}} (\log n)^{-(1-\nu)/(2p)},$$

which is as desired. \square

2.3. Comparison with MC and QMC. We first discuss the implications of Theorem 4 with regards to MC methods. Using the law of iterated logarithms (see, e.g., [29]), one can show that the error convergence rate for MC is bounded a.s. by $\mathcal{O}(n^{-1/2} \sqrt{\log \log n})$. Comparing this with Theorem 4, it is clear that, for *fixed* dimension p , the error rate of support points is *asymptotically* quicker than MC by a poly-log factor. This is reflected in the simulations of Section 4, where support points enjoy a sizable improvement

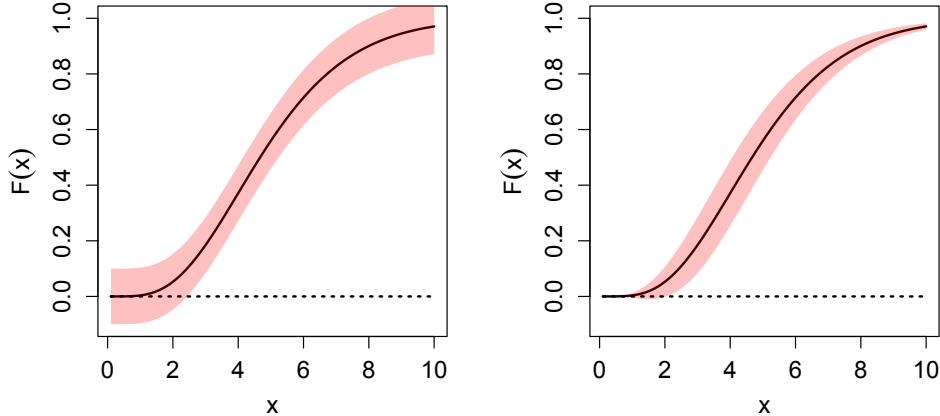


Figure 2: Uniform (left) and non-uniform (right) error bands for $F_{W_n}(x)$. $F_{W_\infty}(x)$ is marked by the black curve.

over MC not only asymptotically, but *for any choice of n* tested. When p is allowed to vary, however, these rates suggest that MC methods *may* have a practical advantage over support points for high-dimensional problems. This is because the MC rate is *independent* of p , whereas the constant $C_{\nu,p}$ in (11) can grow rapidly in p . This *curse-of-dimensionality* is, however, not observed from simulations, where support points enjoy a notable error reduction over MC for both low and moderate p .

Compared to QMC, the existence rate in Theorem 4 falls short. To see this, assume the standard QMC setting of $F = U[0, 1]^p$. For *fixed* p , one can show [19] that for any integrand g with bounded variation (in the sense of Hardy and Krause), the error convergence for classical QMC point sets is $\mathcal{O}(n^{-1}(\log n)^p)$, which is faster than the rate in (11). Second, when p is allowed to vary, it can be shown that *randomized* QMC (RQMC) methods, e.g., the *randomly-shifted lattice rules* in [53] or *randomized Sobol' sequences* in [46], enjoy the same relief from dimensionality as MC. This *lifting* of the curse-of-dimensionality is demonstrated in the breakthrough paper [32], who proved that under certain regularity conditions on g , the *averaged* error for RQMC can be bounded by $\mathcal{O}(C_\nu n^{-1+\nu})$ for any $\nu \in (0, 1/2]$. The key here is that the constant C_ν does not depend on p , allowing the averaged error to be sufficiently bounded in *any dimension* p . To contrast, the existence rate in Theorem 4 does not enjoy this property, since $C_{\nu,p}$ may depend on p .

Fortunately, the simulations in Section 4 tell a different story: for nearly

all point set sizes n tested, support points enjoy *sizable* improvements over both MC and RQMC, for both low and moderate dimensions! This suggests the rate in Theorem 4 may be far from tight. One likely culprit is the use of a *uniform* Barry-Esseen-like rate for degenerate V-statistics in Lemma 4. As the left plot of Figure 2 illustrates, this rate gives the same error bound for $F_{W_n}(x)$ over *all* values of x , whereas the *non-uniform* rate in the right plot provides a larger bound for values of x near the median, and a smaller bound near the tails. Since the integration error relies on only the left tail of $F_{W_n}(x)$ as $x \rightarrow 0^+$, a non-uniform bound can provide a considerable improvement to the rate in Theorem 4! Although we have found no existing work on such a rate for *degenerate* V-statistics, there has been recent and exciting work in a similar vein for *non-degenerate* V-statistics. In particular, page 84 of [11] suggests the following non-uniform bound may be attainable for our application: for any $\alpha > 1$, $\exists b'_{\alpha,p}, d'_{\alpha,p} > 0$ such that:

$$(21) \quad |F_{W_n}(x) - F_{W_\infty}(x)| \leq b'_{\alpha,p} n^{-1/2} (\log n)^{\alpha-1} \exp\{-d'_{\alpha,p}(x + \gamma_n)^{-1/(\alpha-1)}\},$$

for some sequence $(\gamma_n)_{n=1}^\infty$. This leads to the following conjecture:

CONJECTURE 1. *Let α be as in the proof of Theorem 4, and suppose (21) holds with $d_{\nu,p} \leq d'_{\alpha,p}$ and $\gamma_n = \mathcal{O}(n^{-\eta})$ for some $\eta > 0$. The existence rate in Theorem 3 can be refined to:*

$$I(g; F, F_n) \leq \sqrt{V(g) C'_{\eta,p}} n^{-(1-\eta)/2}.$$

The proof for this follows verbatim as that for Theorem 4 from (20). Specifically, setting (21) equal to the right-hand side of (19) and solving for x , we get $x^* \leq C'_{\eta,p} n^{-\eta}$, which provides the conjectured rate. Note that for $\eta \geq 1$, the conjectured rate allows support points to be more competitive theoretically with QMC for fixed p . Exploring the dependency on p for constants may also reveal hints on the apparent relief from dimensionality observed for support points in simulations.

To summarize, while the existence rate in Theorem 4 serves its purpose in illustrating the advantage of support points over MC, simulations suggest that this rate is far from tight. The proof technique presented, however, appears to be valuable for future work, and recent developments in probability suggest that support points may be theoretically competitive with QMC.

3. Generating support points. A key appeal for support points is the efficiency by which these point sets can be computed, made possible by exploiting the rich optimization structure of the energy distance. In this

section, we present two algorithms, `sp.bcd` and `sp.sbcd`, which employ blockwise coordinate descent (BCD) and/or resampling to quickly compute support points. The choice to use one algorithm over the other depends on how easily samples can be generated from F : `sp.bcd` should be used when samples are computationally expensive to obtain, and `sp.sbcd` should be used otherwise. We then prove the correctness of both algorithms in terms of convergence to a stationary point set, and briefly discuss its running times.

3.1. Algorithm statements. We first present the steps for `sp.bcd`, then introduce `sp.sbcd` as an improvement on `sp.bcd` when multiple sample batches from F are readily available. Suppose a single sample batch $\{\mathbf{y}_m\}_{m=1}^N$ is obtained from the desired distribution F . Using this, `sp.bcd` optimizes the following *Monte Carlo estimate* of the support points formulation (O):

$$(MC) \quad \underset{\mathbf{x}_1, \dots, \mathbf{x}_n}{\operatorname{argmin}} \hat{E}(\{\mathbf{x}_i\}; \{\mathbf{y}_m\}) \equiv \frac{2}{nN} \sum_{i=1}^n \sum_{m=1}^N \|\mathbf{y}_m - \mathbf{x}_i\|_2 - \frac{1}{n^2} \sum_{i=1}^n \sum_{j=1}^n \|\mathbf{x}_i - \mathbf{x}_j\|_2.$$

For goodness-of-fit testing, \hat{E} was proposed by [59] as a two-sample statistic for testing whether $\{\mathbf{y}_m\}_{m=1}^N$ and $\{\mathbf{x}_i\}_{i=1}^n$ are generated from the same distribution. As an optimization problem, however, the goal is to *recover* an optimal point set $\{\boldsymbol{\xi}_i\}_{i=1}^n$ which best represents (in a distributional sense) the random sample $\{\mathbf{y}_m\}_{m=1}^N$ from F .

Clearly, a black-box optimization of (MC) (e.g., gradient descent methods with line-search) is computationally intractable even for small n and p , since a *single evaluation* of either both objective and gradient requires $\mathcal{O}(Nnp)$ work. Upon a closer inspection, \hat{E} can be written as a difference of convex (d.c.) functions in $\mathbf{x} = (\mathbf{x}_1, \dots, \mathbf{x}_n)$, namely, the two terms in (MC). This suggests that the problem can be solved using d.c. programming methods, which enjoy a well-established theoretical and numerical framework and allow for *global optimization* (see [63] and [60] for a detailed review). Unfortunately, as discussed in Section 5, the work required for existing d.c. methods is computationally intractable for generating even a *small* number of support points in *low* dimensions. A more efficient method is therefore needed to highlight the practical applicability of support points.

Luckily, \hat{E} also exhibits nice *blockwise* structure, which we exploit using a technique called *blockwise coordinate descent*. The idea behind BCD is as follows. Applied to (MC), this method updates each point \mathbf{x}_i as the blockwise optimization solution of (MC) when the other $n - 1$ points are fixed, then cyclically repeats this procedure until the point set converges. In statistics and machine learning, BCD is used extensively for solving high-dimensional learning problems, such as LASSO [22] and graph estimation

[21], due to its linear running time in p . Similarly, we show later that `sp.bcd` and `sp.sbcd` can efficiently generate high-quality support points in practice, with computation time growing *linearly* in point set size n and dimension p . This efficiency comes at a cost though, since the proposed algorithms provide only *stationary* solutions instead of *globally optimal* ones. Nonetheless, we show in Section 4 that these stationary point sets can provide considerable improvements over MC and QMC in integration.

One requirement for BCD is that the objective needs to be continuously differentiable, because non-differentiability can cause the BCD iterations to fail to converge to a limit (see, e.g., page 94 of [2]). To this end, we employ the *smoothed* L_2 -norm $d_\epsilon(\mathbf{x}, \mathbf{y}) = \sqrt{\|\mathbf{x} - \mathbf{y}\|_2^2 + \epsilon}$ in place of $\|\cdot\|_2$, which removes the non-differentiability of the latter at $\mathbf{0}$. Applied to (MC), this gives the *smoothed MC* formulation:

$$(SMC) \quad \underset{\mathbf{x}_1, \dots, \mathbf{x}_n}{\operatorname{argmin}} \hat{E}_\epsilon(\{\mathbf{x}_i\}; \{\mathbf{y}_m\}) \equiv \frac{2}{nN} \sum_{i=1}^n \sum_{m=1}^N d_\epsilon(\mathbf{y}_m, \mathbf{x}_i) - \frac{1}{n^2} \sum_{i=1}^n \sum_{j=1}^n d_\epsilon(\mathbf{x}_i, \mathbf{x}_j).$$

When $\epsilon \rightarrow 0^+$, the formulation (MC) can be recovered. To foreshadow, the proposed algorithms will successively decrease the smoothing parameter ϵ , allowing point set iterates to converge to a stationary solution of the unsmoothed formulations.

Fixing the other $n - 1$ points, the blockwise optimization of \mathbf{x}_i becomes:

$$(22) \quad \underset{\mathbf{x}}{\operatorname{argmin}} \hat{E}_{i,\epsilon}(\mathbf{x}; \{\mathbf{x}_j\}, \{\mathbf{y}_m\}) \equiv \frac{1}{N} \sum_{m=1}^N d_\epsilon(\mathbf{y}_m, \mathbf{x}) - \frac{1}{n} \sum_{j=1, j \neq i}^n d_\epsilon(\mathbf{x}, \mathbf{x}_j).$$

Similar to before, black-box gradient descent methods are highly inefficient here, since line-searches require multiple objective and gradient evaluations within a single iteration. We instead employ a majorization-minimization (Mm) iterative scheme [33] which exploits the distance-based d.c. structure of the blockwise problem (22). Mm consists of two steps: obtaining a surrogate function which majorizes $\hat{E}_{i,\epsilon}$ (defined later) at the current iterate, then updating the next iterate as the minimizer of this surrogate. The secret for computational speed-up is to find a surrogate with a *closed-form* minimizer which can be easily evaluated. To this end, we will derive a quadratic maximizer for $\hat{E}_{i,\epsilon}$, allowing (22) to be optimized in time linear in p . This linear time is crucial for the efficiency of the overall method, since the blockwise problem needs to be solved n times for *each* BCD cycle.

Algorithm 1 summarizes the detailed steps for `sp.bcd` following the developments above. We will prove in the next subsection that `sp.bcd` converges to a stationary solution of (MC), with running time for each BCD cycle linear

Algorithm 1 `sp.bcd` [`sp.sbcd`] for generating support points.

- Sample $\mathcal{D}_0 = \{\mathbf{x}_i\}_{i=1}^n$ from $\{\mathbf{y}_m\}_{m=1}^N$. [Sample $\mathcal{D}_0 = \{\mathbf{x}_i\}_{i=1}^n \stackrel{i.i.d.}{\sim} F$.]
- Set $f_\epsilon = \hat{E}_\epsilon$. [Set $f_\epsilon = E_\epsilon$.] Initialize $\psi > 0$, $\tau \in (0, 1)$ and $\epsilon_0 > 0$.
- Set $k = 0$, and **repeat** until convergence:
 - **BCD:** Set $\epsilon \leftarrow \epsilon_k$, and **repeat** until $\|\nabla f_\epsilon(\mathcal{D}_k)\| < \psi\epsilon$:
 - **For** $i = 1, \dots, n$ **do**:
 - * Set $\mathbf{x}^{[0]} \leftarrow \mathbf{x}_i$.
 - * **Mm:** Set $l = 0$, and **repeat** until convergence of $\mathbf{x}^{[l]}$:
 - Set $\mathbf{x}^{[l+1]} \leftarrow M_i(\mathbf{x}^{[l]}; \{\mathbf{x}_j\}, \{\mathbf{y}_m\}, \epsilon)$, with M_i defined in (25).
 - [Set $\mathbf{x}^{[l+1]} \leftarrow M_i(\mathbf{x}^{[l]}; \{\mathbf{x}_j\}, \{\mathbf{y}_m^{[l]}\}, \epsilon)$, where $\{\mathbf{y}_m^{[l]}\}_{m=1}^N \stackrel{i.i.d.}{\sim} F$.]
 - Update $l \leftarrow l + 1$.
 - * Set $\mathbf{x}_i \leftarrow \mathbf{x}^{[l]}$.
 - Update $\mathcal{D}_k \leftarrow \{\mathbf{x}_i\}_{i=1}^n$.
 - Set $\epsilon_{k+1} \leftarrow \tau\epsilon_k$, and update $k \leftarrow k + 1$.
 - Return $\mathcal{D}_\infty = \{\mathbf{x}_i\}_{i=1}^n$.

in n and p . One caveat for `sp.bcd` is that it uses only *one* sample batch from F , even when samples can be generated efficiently from F . This motivates the second algorithm, `sp.sbcd`, whose steps are bracketed in Algorithm 1. The main contribution for `sp.sbcd` is that the approximating sample $\{\mathbf{y}_m\} \sim F$ is *resampled* within *each* Mm iteration (a procedure known as *stochastic Mm*). As we show below, this resampling scheme allows `sp.sbcd` to converge to a stationary point set for the *desired* formulation (O).

3.2. *Algorithmic convergence.* Assume $\mathcal{X} \subseteq \mathbb{R}^p$ is compact for the following discussion, and define the *expected analogue* of (SMC):

$$(S) \quad \underset{\mathbf{x}_1, \dots, \mathbf{x}_n}{\operatorname{argmin}} E_\epsilon(\{\mathbf{x}_i\}) \equiv \frac{2}{n} \sum_{i=1}^n \mathbb{E}[d_\epsilon(\mathbf{Y}, \mathbf{x}_i)] - \frac{1}{n^2} \sum_{i=1}^n \sum_{j=1}^n d_\epsilon(\mathbf{x}_i, \mathbf{x}_j), \quad \mathbf{Y} \sim F,$$

and its blockwise problem:

$$(23) \quad \underset{\mathbf{x}}{\operatorname{argmin}} E_{i,\epsilon}(\mathbf{x}; \{\mathbf{x}_j\}) \equiv \mathbb{E}[d_\epsilon(\mathbf{Y}, \mathbf{x})] - \frac{1}{n} \sum_{j=1, j \neq i}^n d_\epsilon(\mathbf{x}, \mathbf{x}_j).$$

We first demonstrate, *for fixed* ϵ , the correctedness of `sp.bcd` and `sp.sbcd` for (SMC) and (S) respectively, then show that under the proposed decrease scheme on ϵ_k , these algorithms return stationary solutions for (MC) and (O).

3.2.1. *Inner loop - Mm.* Consider first the Mm inner loop in `sp.bcd` and `sp.sbcd`, which solves the blockwise problems (22) and (23), respectively. For clarity, we provide an overview of Mm below, following [33].

DEFINITION 4. *Let $f : \mathbb{R}^p \rightarrow \mathbb{R}$ be the objective function to be minimized. A function $h(\mathbf{x}|\mathbf{x}')$ majorizes $f(\mathbf{x})$ at a point $\mathbf{x}' \in \mathbb{R}^p$ if:*

$$(24) \quad h(\mathbf{x}'|\mathbf{x}') = f(\mathbf{x}') \quad \text{and} \quad h(\mathbf{x}|\mathbf{x}') \geq f(\mathbf{x}) \quad \forall \mathbf{x} \neq \mathbf{x}'.$$

Starting at an initial point $\mathbf{x}^{[0]}$, the goal in Mm is to minimize the majorizing surrogate function h in place of the true objective f , and iterate the updates $\mathbf{x}^{[t+1]} \leftarrow \operatorname{argmin}_{\mathbf{x}} h(\mathbf{x}|\mathbf{x}^{[t]})$ until convergence. Using these updates, the so-called *descent property* $f(\mathbf{x}^{[t+1]}) \leq f(\mathbf{x}^{[t]})$ can be easily be shown, which ensures solution iterates are always decreasing in f .

The trick for computational efficiency is to find a majorizing function g with an easy-to-evaluate, closed-form minimizer. The following lemma and theorem show that such a majorizer is attainable by exploiting the *distance-based structure* of $\hat{E}_{i,\epsilon}$.

LEMMA 7. $h(\mathbf{x}|\mathbf{x}') = \frac{\|\mathbf{x}\|_2^2}{2\|\mathbf{x}'\|_2} + \frac{\|\mathbf{x}'\|_2}{2}$ majorizes $\|\mathbf{x}\|_2$ at \mathbf{x}' for any $\mathbf{x}' \in \mathbb{R}^p$.

PROOF. Clearly, $h(\mathbf{x}'|\mathbf{x}') = \|\mathbf{x}'\|_2$. When $\mathbf{x} \neq \mathbf{x}'$, note that:

$$(\|\mathbf{x}\|_2 - \|\mathbf{x}'\|_2)^2 = \|\mathbf{x}\|_2^2 + \|\mathbf{x}'\|_2^2 - 2\|\mathbf{x}\|_2\|\mathbf{x}'\|_2 \geq 0 \Rightarrow \|\mathbf{x}\|_2^2 + \|\mathbf{x}'\|_2^2 \geq 2\|\mathbf{x}\|_2\|\mathbf{x}'\|_2,$$

so $h(\mathbf{x}|\mathbf{x}') = \frac{\|\mathbf{x}\|_2^2}{2\|\mathbf{x}'\|_2} + \frac{\|\mathbf{x}'\|_2}{2} = \frac{\|\mathbf{x}\|_2^2 + \|\mathbf{x}'\|_2^2}{2\|\mathbf{x}'\|_2} \geq \frac{2\|\mathbf{x}'\|_2\|\mathbf{x}\|_2}{2\|\mathbf{x}'\|_2} = \|\mathbf{x}\|_2$. \square

Lemma 7 yields the following appealing geometric interpretation. When $p = 1$, $\|\mathbf{x}\|_2$ becomes $|x|$, and the majorizing function $h(x|x')$ can be seen as the tightest convex quadratic function intersecting $|x|$ at the point x' . For $p > 1$, $\|\mathbf{x}\|_2$ can be seen as a second-order cone centered at $\mathbf{0}$, with $h(\mathbf{x}|\mathbf{x}')$ being the tightest convex paraboloid intersecting this cone at \mathbf{x}' .

Using this lemma, the following theorem presents a *quadratic* majorizer for the blockwise objective $\hat{E}_{i,\epsilon}$. It is worth noting that the *quadratic* nature of this majorizer is a direct consequence of the *L_2 -distance* employed in the energy criterion. This is paramount for the efficient optimization of the blockwise problem (22), since its minimizer can be computed in time linear in n and p .

THEOREM 5. Define $h_i(\mathbf{x}|\mathbf{x}')$ as:

$$h_i(\mathbf{x}|\mathbf{x}') = \frac{1}{N} \sum_{m=1}^N \left(\frac{\|\mathbf{x} - \mathbf{y}_m\|_2^2}{2d_\epsilon(\mathbf{x}', \mathbf{y}_m)} + \zeta_m \right) - \frac{1}{n} \sum_{j=1, j \neq i}^n \left(d_\epsilon(\mathbf{x}', \mathbf{x}_j) + \frac{(\mathbf{x}' - \mathbf{x}_j)^T(\mathbf{x} - \mathbf{x}')}{d_\epsilon(\mathbf{x}', \mathbf{x}_j)} \right),$$

where $\zeta_m \equiv d_\epsilon(\mathbf{y}_m, \mathbf{x}') - \|\mathbf{x}' - \mathbf{y}_m\|_2^2 / (2d_\epsilon(\mathbf{x}', \mathbf{y}_m))$ is a constant ensuring $h_i(\mathbf{x}'|\mathbf{x}') = \hat{E}_{i,\epsilon}(\mathbf{x}')$. Then $h_i(\mathbf{x}|\mathbf{x}')$ majorizes $\hat{E}_{i,\epsilon}(\mathbf{x})$ at $\mathbf{x} = \mathbf{x}'$, and the global minimizer of $h_i(\mathbf{x}|\mathbf{x}')$ becomes:

$$(25) \quad M_i(\mathbf{x}'; \{\mathbf{x}_j\}, \{\mathbf{y}_m\}, \epsilon) \equiv \left(\sum_{m=1}^N d_\epsilon(\mathbf{x}', \mathbf{y}_m)^{-1} \right)^{-1} \left(\frac{N}{n} \sum_{j=1, j \neq i}^n \frac{\mathbf{x}' - \mathbf{x}_j}{d_\epsilon(\mathbf{x}', \mathbf{x}_j)} + \sum_{m=1}^N \frac{\mathbf{y}_m}{d_\epsilon(\mathbf{x}', \mathbf{y}_m)} \right)$$

PROOF. Using Lemma 7 and algebraic manipulations, it is easy to show that the first term in $h_i(\mathbf{x}|\mathbf{x}')$ majorizes the first term in $\hat{E}_{i,\epsilon}(\mathbf{x})$ at $\mathbf{x} = \mathbf{x}'$. Since the second term in $\hat{E}_{i,\epsilon}(\mathbf{x})$ is concave, a linearization at $\mathbf{x} = \mathbf{x}'$ provides a majorization function at \mathbf{x}' , which is precisely the second term in $h_i(\mathbf{x}|\mathbf{x}')$. This provides the first part of the claim.

For the second part, consider the quadratic function $\sum_{m=1}^N \frac{a_m}{2} \|\mathbf{x} - \mathbf{y}_m\|_2^2 - \sum_{j=1}^n \mathbf{c}_j^T (\mathbf{x} - \mathbf{x}') + K$, where $a_m > 0$ and $K \in \mathbb{R}$. Setting its gradient to $\mathbf{0}$ and invoking convexity, the minimizer becomes $[\sum_{m=1}^N a_m]^{-1} (\sum_{j=1}^n \mathbf{c}_j + \sum_{m=1}^N a_m \mathbf{y}_m)$. Applying this proves the assertion. \square

We can then prove the Mm inner loop converges to a stationary point.

COROLLARY 2. (Mm convergence - **sp.bcd**) For any $\mathbf{x}^{[0]}$ and fixed sample $\{\mathbf{y}_m\}$, the sequence $\mathbf{x}^{[l+1]} = M_i(\mathbf{x}^{[l]}; \{\mathbf{x}_j\}, \{\mathbf{y}_m\}, \epsilon)$ converges to a limit point $\mathbf{x}^{[\infty]}$ satisfying $\nabla \hat{E}_{i,\epsilon}(\mathbf{x}^{[\infty]}) = \mathbf{0}$. Moreover, applying $L_i = \mathcal{O}(\log \delta^{-1})$ iterations of M_i ensures $\|\hat{E}_{i,\epsilon}(\mathbf{x}^{[l]}) - \hat{E}_{i,\epsilon}(\mathbf{x}^{[\infty]})\|_2 < \delta$.

COROLLARY 3. (Mm convergence - **sp.sbcd**) For any $\mathbf{x}^{[0]}$ and $\{\mathbf{y}_m^{[l]}\}_{m=1}^N \stackrel{i.i.d.}{\sim} F$, the sequence $\mathbf{x}^{[l+1]} = M_i^{[l]}(\mathbf{x}^{[l]})$, with $M_i^{[l]}(\cdot) \equiv M_i(\cdot; \{\mathbf{x}_j\}, \{\mathbf{y}_m^{[l]}\}, \epsilon)$, converges a.s. to a limit point $\mathbf{x}^{[\infty]}$ satisfying $\nabla \hat{E}_{i,\epsilon}(\mathbf{x}^{[\infty]}) = \mathbf{0}$.

PROOF. (Corollary 2) Since $h_i(\mathbf{x}|\mathbf{x}')$ majorizes $\hat{E}_{i,\epsilon}(\mathbf{x})$ at $\mathbf{x} = \mathbf{x}'$, with $g_i(\mathbf{x}|\mathbf{x}')$ continuous in $(\mathbf{x}, \mathbf{x}')$ and $\nabla_{\mathbf{x}} h_i(\mathbf{x}'|\mathbf{x}') = \nabla_{\mathbf{x}} \hat{E}_{i,\epsilon}(\mathbf{x}')$, Theorem 1 in [49] guarantees $\{\mathbf{x}^{[l]}\}_{l=1}^\infty$ converges to a limit point $\mathbf{x}^{[\infty]}$ with $\nabla \hat{E}_{i,\epsilon}(\mathbf{x}^{[\infty]}) = \mathbf{0}$.

As for its convergence rate, it can be shown (e.g., pg. 301 of [45]) that:

$$\lim_{l \rightarrow \infty} \frac{\|\hat{E}_{i,\epsilon}(\mathbf{x}^{[l+1]}) - \hat{E}_{i,\epsilon}(\mathbf{x}^{[\infty]})\|_2}{\|\hat{E}_{i,\epsilon}(\mathbf{x}^{[l]}) - \hat{E}_{i,\epsilon}(\mathbf{x}^{[\infty]})\|_2} = \lambda$$

where $\lambda \in (0, 1)$ is the largest absolute eigenvalue of $\mathbf{I} - [\nabla^2 h_i(\mathbf{x}^{[\infty]}|\mathbf{x}^{[\infty]})]^{-1} \nabla^2 \hat{E}_{i,\epsilon}(\mathbf{x}^{[\infty]})$. This implies $\mathcal{O}(\log \delta^{-1})$ iterations are sufficient for ensuring $\|\hat{E}_{i,\epsilon}(\mathbf{x}^{[l]}) - \hat{E}_{i,\epsilon}(\mathbf{x}^{[\infty]})\|_2 < \delta$. \square

PROOF. (Corollary 3) Under regularity conditions, Prop. 3.4 of [37] shows that a stationary point can be obtained for the expected blockwise objective $E_{i,\epsilon}$ by repeatedly applying Mm updates on *Monte Carlo estimates* of $E_{i,\epsilon}$, where the approximating samples $\{\mathbf{y}_m^{[l]}\}$ are independently generated within each update. These conditions are satisfied by the compactness of \mathcal{X} and the existence of *directional derivatives* for $\hat{E}_{i,\epsilon}$ and $E_{i,\epsilon}$, so the claim holds. \square

Putting everything together, the inner Mm loop for `sp.bcd` solves the blockwise problem (22) to an objective gap of δ (from a stationary point) in $\mathcal{O}(Np \log \delta^{-1})$ time, since a total of $L_i = \mathcal{O}(\log \delta^{-1})$ Mm iterations is needed, each requiring $\mathcal{O}(Np)$ work. Although a similar rate is difficult to establish for `sp.sbcd` due to its stochastic nature, simulation studies (not reported for brevity) show that its convergence behavior is very similar to `sp.sbd`.

3.2.2. *Middle loop - BCD*. To establish the correctedness of the outer BCD loop, one needs to prove *descent* and *closedness* of the Mm algorithmic map for both `sp.bcd` and `sp.sbcd`. This is addressed below.

LEMMA 8. (Descent - `sp.bcd`) Define the Mm algorithmic map $S_i = \circ_{l=1}^{L_i} M_i$, where $1 \leq L_i < \infty$ and M_i is defined in Corollary 2. Then $\nabla \hat{E}_{i,\epsilon}(\mathbf{x}) = \mathbf{0} \Rightarrow S_i(\mathbf{x}) = \mathbf{x}$ and $\nabla \hat{E}_{i,\epsilon}(\mathbf{x}) \neq \mathbf{0} \Rightarrow \hat{E}_{i,\epsilon}[S_i(\mathbf{x})] < \hat{E}_{i,\epsilon}(\mathbf{x})$ for any $\mathbf{x} \in \mathcal{X}$.

PROOF. By construction, $\nabla \hat{E}_{i,\epsilon}(\mathbf{x}) = \nabla h_i(\mathbf{x}|\mathbf{x})$. If $\nabla \hat{E}_{i,\epsilon}(\mathbf{x}) = \mathbf{0}$, then we have $S_i(\mathbf{x}) = \mathbf{x}$ by strong convexity of h_i . Conversely, if $\nabla \hat{E}_{i,\epsilon}(\mathbf{x}) \neq \mathbf{0}$, then, since $M_i(\mathbf{x})$ is the global minimizer of $h_i(\cdot|\mathbf{x})$, it follows by the descent property of Mm that $\hat{E}_{i,\epsilon}(M_i(\mathbf{x})) \leq h_i(M_i(\mathbf{x})|\mathbf{x}) < h_i(\mathbf{x}|\mathbf{x}) = \hat{E}_{i,\epsilon}(\mathbf{x})$. Repeating this argument for $L_i < \infty$ iterations proves the claim. \square

Unfortunately, due to its stochasticity, one cannot guarantee the same descent property for `sp.sbcd` with certainty. The following assumption is therefore needed:

ASSUMPTION 1. (Descent - `sp.sbcd`) Define the map $S_i = \circ_{l=1}^{L_i} M_i^{[l]}$, where $0 \leq L_i < \infty$ and $M_i^{[l]}$ is defined in Corollary 3. Then $\nabla E_{i,\epsilon}(\mathbf{x}) = \mathbf{0} \Rightarrow M_i(\mathbf{x}) = \mathbf{x}$ and $\nabla E_{i,\epsilon}(\mathbf{x}) \neq \mathbf{0} \Rightarrow E_{i,\epsilon}[S_i(\mathbf{x})] < E_{i,\epsilon}(\mathbf{x})$ for any $\mathbf{x} \in \mathcal{X}$.

Assumption 1 has two parts: (a) the Mm procedure should not update when the initial point \mathbf{x} is stationary, i.e., $\nabla E_{i,\epsilon}(\mathbf{x}) = \mathbf{0}$, and (b) the point $S_i(\mathbf{x})$ returned by Mm should have a strictly smaller objective than \mathbf{x} when \mathbf{x} is non-stationary. In practice, this assumption can be *enforced* as follows. First, a large Monte Carlo sample can be used to check the initial condition

$\nabla E_{i,\epsilon}(\mathbf{x}) = \mathbf{0}$ and the termination condition $E_{i,\epsilon}[S_i(\mathbf{x})] < E_{i,\epsilon}(\mathbf{x})$. When the initial condition holds, L_i is set as 0, whereas when the termination condition does not hold, the Mm loop is repeated until a strict decrease is observed for $E_{i,\epsilon}$. Second, setting a larger resampling size N allows the *estimated majorizer* to better approximate the *true majorizer* for $E_{i,\epsilon}$, which in turn provides a higher probability for the termination condition to be satisfied. However, there is a trade-off: a larger N also incurs more work for Mm. In our simulations, the choice of $N = 10,000$ appears to work quite well.

LEMMA 9. (Closedness) Define the map $S : \mathbb{R}^{2np} \rightarrow \mathbb{R}^{np}$ as:

$$(26) \quad [(\mathbf{x}_1, \dots, \mathbf{x}_n), (\mathbf{0}_{(i-1)p}, \mathbf{1}_p, \mathbf{0}_{(n-i)p})] \mapsto (\mathbf{x}_1, \dots, \mathbf{x}_{i-1}, S_i(\mathbf{x}_i), \dots, \mathbf{x}_n),^1$$

where S_i is defined in Lemma 8 and Assumption 1, respectively. Then S is closed for $\Gamma = \{(\mathbf{x}, \mathbf{d}) : \nabla f_\epsilon(\mathbf{x}) \neq \mathbf{0}\}$, where $f_\epsilon = \hat{E}_\epsilon$ for `sp.bcd` and $f_\epsilon = E_\epsilon$ for `sp.sbcd`.

PROOF. By definition, a map S is *closed* for Γ if, for all $\mathbf{a} \in \Gamma$, any sequence $\{\mathbf{a}_k\} \subseteq \Gamma$ with $\mathbf{a}_k \rightarrow \mathbf{a}, \mathbf{z}_k \equiv S\mathbf{a}_k \rightarrow \mathbf{z}$ implies $\mathbf{z} = S\mathbf{a}$. Note that this holds whenever S is continuous. Here, S_i is a composition of $L_i < \infty$ continuous maps M_i , so it must itself be continuous and therefore closed. \square

These two properties can then be used to prove convergence of `sp.bcd` and `sp.sbcd` to a *stationary solution* for *fixed* ϵ .

THEOREM 6. For fixed $\epsilon > 0$, `sp.bcd` [`sp.sbcd`] converges to a stationary point set for (SMC) [(S)].

PROOF. Note that one BCD cycle follows the algorithmic map A :

$$A = (SC_n)(SC_{n-1}) \cdots (SC_1),$$

where S is the map in Lemma 9 and C_i is the assignment map for point i :

$$\mathbf{x} = (\mathbf{x}_1, \dots, \mathbf{x}_n) \mapsto [(\mathbf{x}_1, \dots, \mathbf{x}_n), (\mathbf{0}_{(i-1)p}, \mathbf{1}_p, \mathbf{0}_{(n-i)p})].$$

By Lemma 9 and continuity of C_i , S is closed for $\Gamma = \{(\mathbf{x}, \mathbf{d}) : \nabla f(\mathbf{x}) \neq \mathbf{0}\}$. By Corollary 2 in Section 7.7 of [36], A must be a closed map for Γ as well, since all local minima of f are contained in \mathcal{X}^n , which is compact. From Lemma 8, the objective f_ϵ (defined in Lemma 9) is also a continuous descent function for A , since $f_\epsilon(A\mathbf{x}) < f_\epsilon(\mathbf{x})$ whenever $\nabla f_\epsilon(\mathbf{x}) \neq \mathbf{0}$ and $f_\epsilon(A\mathbf{x}) = f_\epsilon(\mathbf{x})$ whenever $\nabla f_\epsilon(\mathbf{x}) = \mathbf{0}$. By the Global Convergence Theorem (Section 7.7 of [36]), `sp.bcd` and `sp.sbcd` (with $\epsilon > 0$ fixed) must generate a point set sequence which converges to a stationary solution for f_ϵ . \square

¹ $\mathbf{0}_q$ and $\mathbf{1}_q$ denote q -vectors of 0's and 1's, respectively.

3.2.3. *Outer loop - ϵ decay.* Finally, we show that the full algorithm for `sp.bcd` and `sp.sbcd` (with decreasing ϵ in Algorithm 1) converges to a stationary solution for the desired problems (MC) and (O), respectively.

THEOREM 7. *Let \mathcal{D}_k be the stationary point set in Algorithm 1 satisfying $\|\nabla f_{\epsilon_k}(\mathcal{D}_k)\| < \psi\epsilon_k$, where f_ϵ is defined in Lemma 9. Then any limiting point set \mathcal{D}_∞ of $\{\mathcal{D}_k\}_{k=1}^\infty$ is Clarke stationary for (MC) [(O)], i.e.:*

$$\mathbf{0} \in \partial f(\mathcal{D}_\infty) \equiv \text{conv}\{\mathbf{v} : \nabla f(\mathcal{D}) \rightarrow \mathbf{v}, f \text{ differentiable at } \mathcal{D}, \mathcal{D} \rightarrow \mathcal{D}_\infty\},$$

where $f = \hat{E}$ for `sp.bcd` [$f = E$ for `sp.sbcd`] and $\text{conv}\{\cdot\}$ denotes the convex hull.

PROOF. Fix $\psi > 0$, $\tau \in (0, 1)$ and $\epsilon_0 > 0$, and let $\epsilon_k = \epsilon_0\tau^k$. From the convergence guarantee in Theorem 6, the stopping condition $\|\nabla f_{\epsilon_k}(\mathcal{D}_k)\| < \psi\epsilon_k$ in Algorithm 1 must be satisfied in finite iterations, since f_ϵ is continuously differentiable. It follows that:

$$\lim_{k \rightarrow \infty} \|\nabla f_{\epsilon_k}(\mathcal{D}_k)\| < \psi \lim_{k \rightarrow \infty} \epsilon_k = 0.$$

Finally, an application of Theorem 1 in [6] shows the gradient consistency condition holds (see [6] for details), which implies $\mathbf{0} \in \partial f(\mathcal{D}_\infty)$, as desired. \square

Similar to Assumption 1, the stopping condition $\|\nabla f_{\epsilon_k}(\mathcal{D}_k)\| < \psi\epsilon_k$ for `sp.sbcd` can be checked using a large Monte Carlo sample from F .

Unfortunately, theoretical running times for `sp.bcd` and `sp.sbcd` are hard to prove, since the iteration count for convergence is difficult to establish for the non-convex objectives \hat{E} and E . However, from Corollary 2, $\mathcal{O}(nNp\log(\delta^{-1}))$ work is required for *one* BCD cycle in `sp.bcd`. Moreover, for all simulations, convergence is achieved in at most 50 BCD cycles and several decreases in ϵ , suggesting that $\mathcal{O}(nNp\log(\delta^{-1}))$ is a good *empirical* estimate of the running times for both `sp.bcd` and `sp.sbcd`. This linearity on n and p allows support points to be efficiently generated for moderate-sized point sets in moderately dimensions, as we show in Section 4.1.

4. Simulation. Here, we present several simulation studies which demonstrate the usefulness of support points in practice. We first discuss the *space-fillingness* of the proposed point sets along with its computation time, then compare its integration performance with MC and RQMC methods. We then propose two important applications for support points. The first is for allocating experimental runs in stochastic simulations, where the goal is to perform uncertainty propagation of input variables. Since input uncertainties

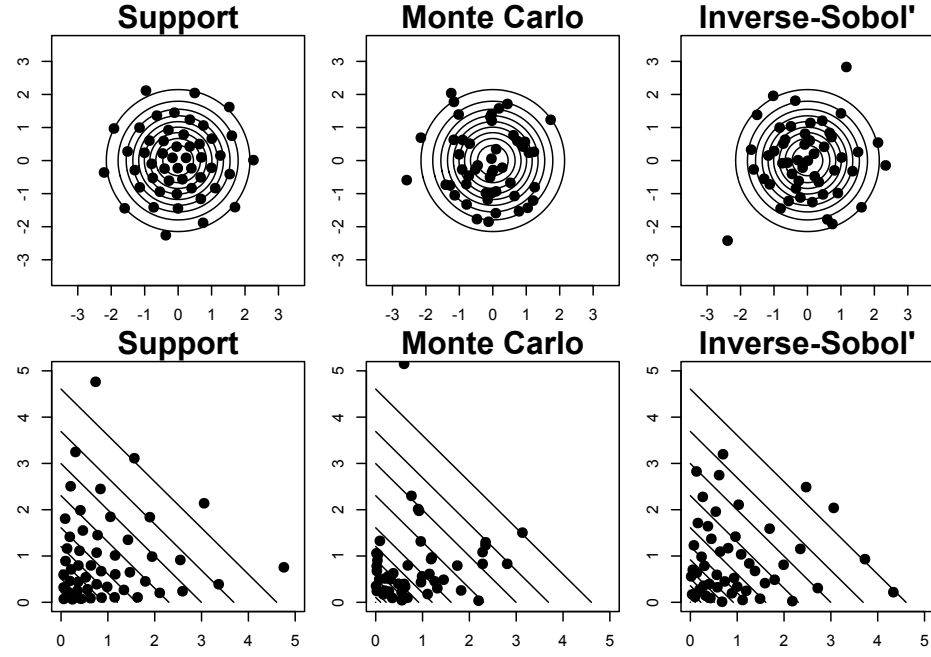


Figure 3: $n = 50$ support points, MC samples and IT-RSS points for i.i.d. $N(0, 1)$ and $\text{Exp}(1)$ in $p = 2$ dimensions. Lines represent density contours.

often follow standard distributions, this highlights the use of `sp.sbcd`. The second is to provide an improved alternative to MCMC thinning for Bayesian computation. Since posterior samples are often computationally expensive to generate, this highlights the use of `sp.bcd`.

4.1. Visualization and timing. We first plot some examples of support points from `sp.sbcd` to illustrate the *space-filling* property of these point sets. Two other point sets are used for comparison: randomly sampled points (i.e., MC) and points from IT-RSS, a QMC method introduced in the next section. Both point sets will later be used to benchmark integration performance.

Figure 3 plots the $n = 50$ point sets for i.i.d. $N(0, 1)$ and $\text{Exp}(1)$ distributions for $p = 2$, with lines representing density contours (additional plots can be found in supplementary materials). From this figure, support points exhibit two appealing features over MC and QMC. First, not only are support points concentrated around regions with higher density, they are also sufficiently *spaced out* from one another to maximize the representative power of each point. We call point sets satisfying these two properties to be *space-filling* on F , a term borrowed from design-of-experiments literature

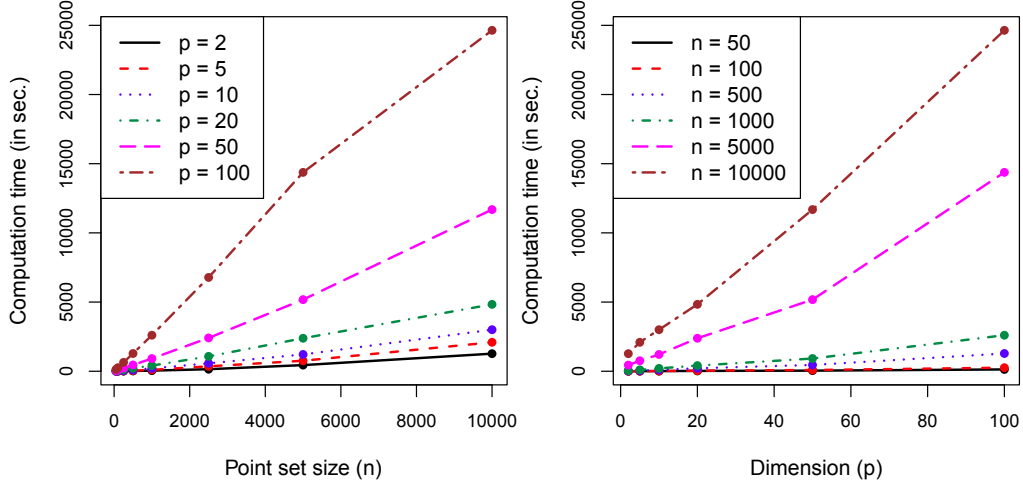


Figure 4: Computation time (in sec.) of support points vs. point set size (n) and dimension (p) for the i.i.d. $N(0, 1)$ distribution.

(see, e.g. [52]) . A key reason for this space-fillingness is the *distance-based* (rather than e.d.f.-based) property of the energy statistic. Specifically, the two terms for $E(F, F_n)$ in (4) force support points to not only mimic the desired distribution F , but also ensures no two points are too close in L_2 -norm. This provides not only a more appealing visual representation of F (see Figure 3), but also more robust integration performance, which we demonstrate later.

Regarding computation time, Figure 4 plots the time required for `sp.sbcd` (in seconds) to generate support points for the i.i.d. $N(0, 1)$ distribution, first as a function of point set size n with fixed dimension p , then as a function of p with fixed n . The resampling size is set at $N = 10,000$, with inner loop tolerance $\delta = 10^{-2}$ and decay settings $(\phi, \tau) = (1, 0.1)$. Similar times are reported for other distributions, and are not reported for brevity. All computations are performed on a single-core Intel Xeon 3.50 Ghz processor. From this figure, two interesting observations can be made. First, these plots give empirical evidence for the linear running time in n and p asserted for `sp.bcd` and conjectured for `sp.sbcd`. Second, as a result of this linear-time algorithm, we see that support points can be efficiently generated for $n \leq 10,000$ and $p \leq 100$. In particular, for $p = 2$, the time required to generate $n = 50 - 10,000$ points ranges from 2 seconds to 20 minutes; for $p = 10$, 8 seconds to 50 minutes; and for $p = 100$, 2 minutes to 6 hours. It should be mentioned that, while the proposed method is more efficient than many existing rep-point methods which employ optimization, its running time is inferior to number-theoretic QMC methods, which can generate, say,

$n = 10^6$ points in $p = 10^3$ dimensions in a matter of seconds. When support points can be generated, however, they can perform significantly better than QMC in integration, as we illustrate next.

4.2. Numerical integration. To investigate the effectiveness of support points for integration, we compare its performance with MC sampling and inverse-transformed randomized Sobol' sequences (IT-RSS). The latter is obtained by first generating a randomized Sobol' sequence using the R package `randtoolbox` [16], then mapping it using an *inverse-transform* of F . As mentioned in Section 2, IT-RSS points are nearly optimal when $F = U[0, 1]^p$, and provide a good benchmark for comparing support points with state-of-the-art QMC techniques. Our simulation set-up is as follows. Support points are generated using `sp.sbcd`, with point set sizes ranging from $n = 50$ to 10,000, and the algorithm parameters N , δ , ϕ and τ set as in Section 4.1. Since MC and IT-RSS are randomized, we replicate both for 100 trials to provide an estimate of error variability (these replications are seeded for reproducibility). Three distributions are considered for F : the i.i.d. $N(0, 1)$, the i.i.d. $Exp(1)$ and the i.i.d. $Beta(2, 4)$ distribution, with p ranging from 2 to 100. Lastly, for the integrand g , two commonly-used test functions are used² from [23]: the Gaussian peak function (GAPK): $g(\mathbf{x}) = \exp\left\{-\sum_{l=1}^p \alpha_l^2 (x_l - u_l)^2\right\}$ and the oscillatory function (OSC): $g(\mathbf{x}) = \cos\left(2\pi u_1 + \sum_{l=1}^p \beta_l x_l\right)$, where $\mathbf{x} = (x_l)_{l=1}^p$ and u_l is the marginal mean for the l -th dimension of F . The scale parameters α_l and β_l are set as $8/p$ and $1/p$, respectively.

Figure 13 plots the resulting log-absolute errors in $p = 5, 10$ and 50 dimensions for the i.i.d. $Exp(1)$ distribution (results are similar for other choices of F , and are deferred to supplementary materials). For MC and IT-RSS, lines indicate the average error decay, while shaded bands mark the area between the 25-th and 75-th error quantiles. Two interesting observations can be made here. First, for nearly all choices of n tested, support points incur considerably reduced errors compared to the averaged performance for both MC and IT-RSS. Indeed, for over half of these cases, support points provide improved performance to even the 25-th error quantile for IT-RSS! This suggests that whenever support points can be generated, they often provide *better integration performance* compared to RQMC. Moreover, while point sets from `sp.sbcd` are not necessarily globally optimal, one sees that they can provide excellent performance in practice. The second observation addresses the theoretical curse-of-dimensionality observed for the existence rate in Theorem 4. From Figure 13, one can see that support points enjoy a distinct

²While the bound in Theorem 3 applies only for polynomials, support points appear to perform quite well for non-polynomial integrands as well, as we show for GAPK and OSC.

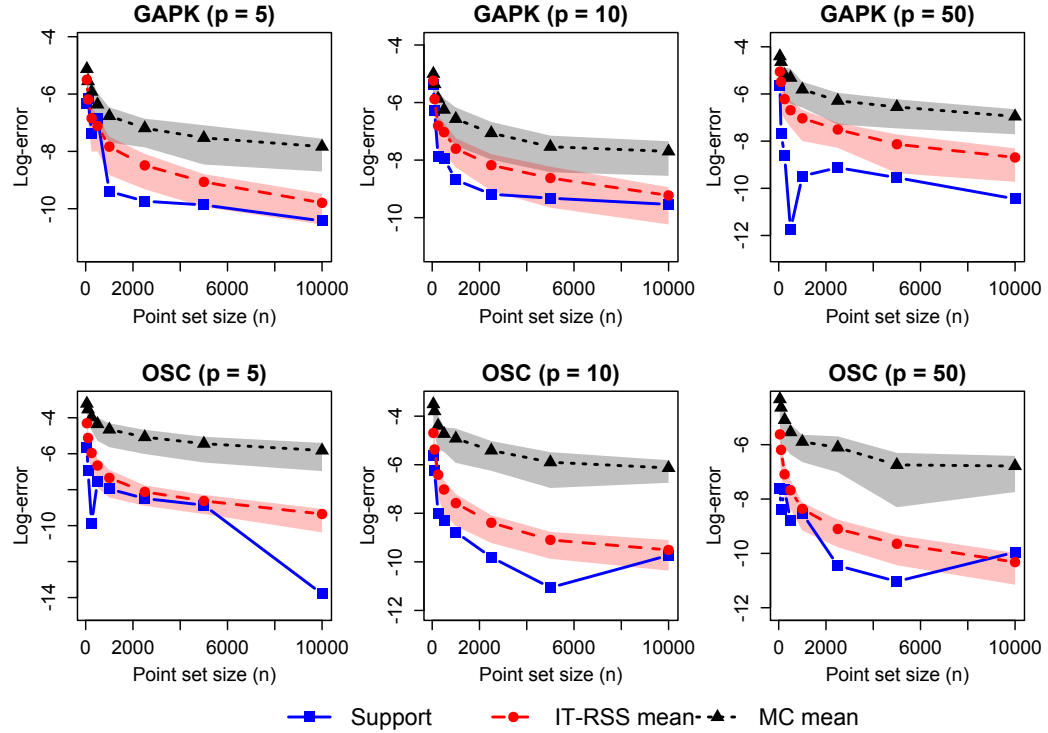


Figure 5: Log-absolute integration errors for the i.i.d. $\text{Exp}(1)$ distribution with $p = 5, 10$ and 50 . Shaded bands mark the region between 25-th and 75-th quantiles.

advantage over MC and IT-RSS in both low and moderate dimensions. In view of the *relief from dimensionality* enjoyed by both randomized methods, this gives some evidence that support points *may* enjoy the same property as well, a much stronger assertion than Theorem 4. Exploring this apparent relief from dimensionality will be an interesting direction for future work.

In summary, for point set sizes of $n \leq 10,000$ in dimensions $p \leq 100$, simulations show support points can be *efficiently generated* and enjoy *improved performance* over MC and RQMC. This allows support points to be applied to many important applications, two of which we describe below.

4.3. Support points for stochastic simulation. We first highlight an important application of support points in simulation. With the development of powerful computational tools, computer simulations are becoming the de-facto method for conducting engineering experiments. For these simulations, an important goal is studying *uncertainty propagation*, or how uncertainty in input variables (e.g., from manufacturing tolerances) propagate and affect

| Input | Distribution |
|-----------------------|-------------------------|
| Borehole radius | $N(0.01, 0.01618)$ |
| Radius of influence | Lognormal(7.71, 1.0056) |
| Upper transmissivity | $U[63070, 115600]$ |
| Upper head | $U[990, 1110]$ |
| Lower transmissivity | $U[63.1, 116]$ |
| Lower head | $U[700, 820]$ |
| Borehole length | $U[1120, 1680]$ |
| Borehole conductivity | $U[9855, 12045]$ |

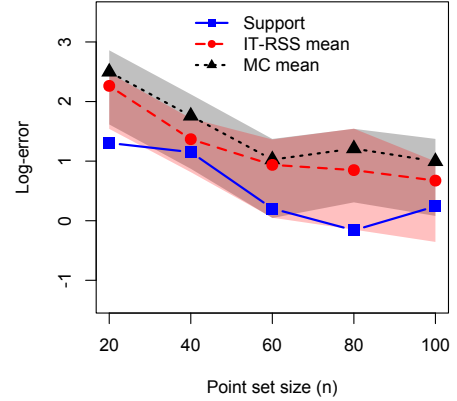


Table 1: Inputs and their uncertainty distributions for the borehole model.

Figure 6: Log-absolute errors for estimating $\mathbb{E}[g(\mathbf{X})]$ in the borehole model.

simulation output. Mathematically, let $g(\mathbf{x})$ be the output observed at input \mathbf{x} , with $\mathbf{X} \sim F$ representing input uncertainties. The distribution $g(\mathbf{X})$ can then be seen as system output uncertainty, and it is of great importance for engineers to estimate this distribution using as few simulation runs as possible, since each run can be computationally and monetarily expensive.

We use the *borehole physical model* [66], which simulates the flow rate of water through a borehole, to demonstrate the effectiveness of support points in this context. Table 1 summarizes the 8 input variables for this model, along with their corresponding uncertainty distributions, which we assume to be independent. To reflect the expensive cost of runs, we test only small point set sizes ranging from $n = 20$ to $n = 100$. Support points are generated using `sp.sbcd` with the same settings as before, with the randomized MC and QMC methods replicated for 100 trials.

We first discuss the estimation of the *expected output* $\mathbb{E}[g(\mathbf{X})]$. Figure 6 plots the log-absolute errors for the three methods, with the shaded band indicating the 25-th and 75-th quantiles for MC and IT-RSS. It can be seen that support points provide the most accurate estimates for all choices of n , illustrating again the improved integration performance of the proposed method to MC and RQMC for small n . Next, to investigate how well these point sets approximate the *output distribution* $g(\mathbf{X})$, Figure 7 compares the estimated densities of $g(\mathbf{X})$ using $n = 80$ points with its true density function, the latter estimated using a large Monte Carlo sample. Visually, the proposed method also provide the best density approximation for $g(\mathbf{X})$, capturing well both the peak and tails of this output distribution. This suggests support points are not only *asymptotically consistent* for density

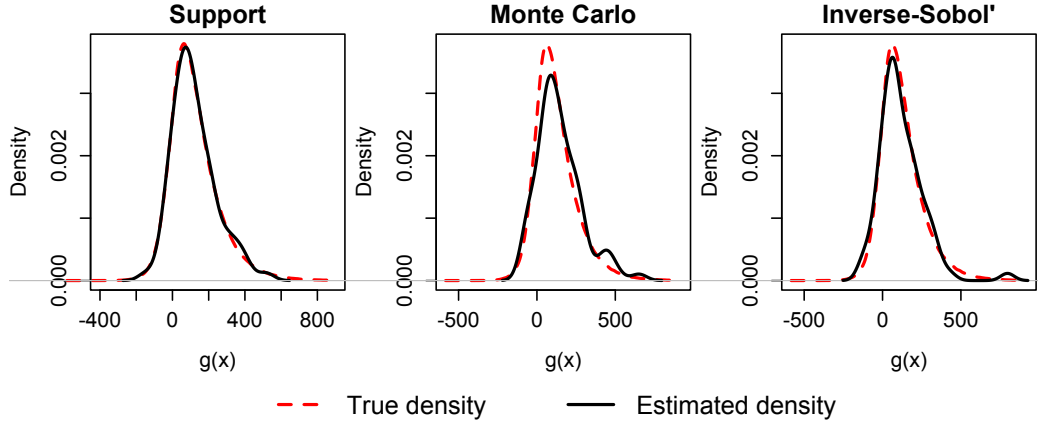


Figure 7: True and estimated density functions for $g(\mathbf{X})$ using $n = 80$ points.

estimation, as demonstrated in Corollary 1(a), but may also be *optimal* in some sense! We look forward to exploring this further in a future paper.

4.4. Support points for Bayesian computation. The second application of support points is as an improved alternative to MCMC thinning for Bayesian computation. *Thinning* here refers to the *discarding of all but every k -th sample* for an MCMC sample chain obtained from the posterior distribution. This is performed for several reasons (see, e.g., [34]): it reduces high autocorrelations in the MCMC chain, saves computer storage space, and reduces processing time for computing derived posterior quantities. However, by carelessly throwing away samples, a glaring fault of thinning is that samples from thinned chains are inherently less accurate than from the full chain. To this end, we show the proposed algorithm `sp.bcd` can provide considerable improvements to thinning by explicitly *optimizing* for a point set which best captures the distribution of the full MCMC chain.

We illustrate this using the orange tree growth model in [15], with a second example on robot arm emulation provided in supplementary materials. The data consists of the trunk circumference measurements $\{Y_i(t_j)\}_{i=1}^5 \}_{j=1}^7$, where $Y_i(t_j)$ denotes the measurement taken on day t_j from tree i . Following [15], the following growth model is assumed:

$$Y_i(t_j) \stackrel{\text{indep.}}{\sim} N(\eta_i(t_j), \sigma_C^2), \quad \eta_i(t_j) = \phi_{i1}/(1 + \phi_{i2} \exp\{\phi_{i3} t_j\}),$$

where ϕ_{i1} , ϕ_{i2} and ϕ_{i3} are model parameters controlling the growth behavior of tree i . There are 16 parameters in total, which we denote by the set

| Parameter | Distribution | $R(\mu, 375)$ | $R(\mu, 750)$ | $R(s, 375)$ | $R(s, 750)$ |
|--------------|---|---------------|---------------|-------------|-------------|
| ϕ_{i1} | $\log \phi_{i1} \stackrel{\text{indep.}}{\sim} N(\mu_1, \sigma_1^2)$ | 2.36 | 2.88 | 15.04 | 6.60 |
| ϕ_{i2} | $\log(\phi_{i2} + 1) \stackrel{\text{indep.}}{\sim} N(\mu_2, \sigma_2^2)$ | 1.77 | 2.24 | 18.25 | 3.11 |
| ϕ_{i3} | $\log(-\phi_{i3}) \stackrel{\text{indep.}}{\sim} N(\mu_3, \sigma_3^2)$ | 1.47 | 2.25 | 11.26 | 119.35 |
| σ_C^2 | $\sigma_C^2 \sim \text{Inv-Gamma}(0.001, 0.001)$ | 0.95 | 2.21 | 6.27 | 8.50 |
| $r(1600)$ | | 1.50 | 2.54 | - | - |
| $r(1625)$ | $r(t) = \frac{1}{5} \sum_{i=1}^5 \frac{\partial}{\partial s} \eta_i(s) \Big _{s=t}$ | 1.56 | 2.54 | - | - |
| $r(1650)$ | | 1.62 | 2.55 | - | - |
| μ_j | $\mu_j \stackrel{\text{i.i.d.}}{\sim} N(0, 100)$ | - | - | - | - |
| σ_j^2 | $\sigma_j^2 \stackrel{\text{i.i.d.}}{\sim} \text{Inv-Gamma}(0.01, 0.01)$ | - | - | - | - |

Table 2: Prior specification for the tree growth model (left), and ratio of thinning over support-point error for posterior quantities (right). $R(\mu, n)$ and $R(s, n)$ denote the error ratio for posterior means and variances using n points, respectively.

$\Theta = (\phi_{11}, \phi_{12}, \dots, \phi_{53}, \sigma^2)$. Since no prior information is available on Θ , we assign vague priors for each parameter, as specified in the left part of Table 2. MCMC sampling is then performed for the posterior distribution using the R package **STAN** [55], with the chain run for 150,000 iterations and the first 75,000 of these discarded as burn-in. The remaining $N = 75,000$ samples are then thinned at a rate of 200 and 100, giving $n = 375$ and $n = 750$ thinned samples, respectively. Support points are generated using **sp.bcd** for the same choices of n , with the full MCMC chain used as the approximating sample $\{\mathbf{y}_m\}_{m=1}^N$. Since posterior variances vary greatly between parameters, we first rescale each parameter in the MCMC chain to unit variances before performing **sp.bcd**, then scale back the resulting support points after.

We then compare how well both thinning and support points estimate the *marginal posterior means and standard deviations* for each parameter, as well as the *averaged instantaneous growth rate* $r(t)$ (see Table 2) at three future times. True posterior quantities are estimated by running a longer MCMC chain with 600,000 iterations. This comparison is summarized in the right part of Table 2, which reports the ratio of thinning over support point error for each parameter. Keeping in mind that a ratio exceeding 1 indicates lower errors for support points, one can see that **sp.bcd** provide a sizable improvement over thinning for nearly all posterior quantities. Again, this should not be surprising, since **sp.bcd** compacts the *full* MCMC chain into a set of *optimal* representative points, whereas thinning wastes valuable information by discarding a majority of this chain. Similar results are reported for the robot arm example in supplementary materials.

5. Conclusion and future work. In this paper, a new method is proposed for compacting a continuous distribution F into a set of representative points called *support points*. These points are defined as the minimizer of the energy distance in [59], and can be viewed as a special type of *energy rep-point*. To justify its use in integration, we proved a Koksma-Hlawka-like result connecting integration error with the energy distance. An existence result is then proved, which demonstrates the quicker convergence of support points over MC. This provides an improvement over the existing energy rep-points in [28] and [3], which suffer from slow convergence rates. To compute support points in practice, the two algorithms `sp.bcd` and `sp.sbcd` are proposed, which can efficiently generate point sets of sizes $n \leq 10,000$ in dimensions $p \leq 100$. Simulations and real-world applications demonstrate the improved performance of support points to both MC and QMC in practice.

As mentioned in Section 3, a promising direction for generating *globally optimal* support points is to view the formulation (O) as a d.c. program. Unfortunately, two key barriers hinder the application of existing d.c. methods here. First, for practical choices of n and p , the formulation (O) is inherently high-dimensional, and, as such, can be computationally intractable for existing methods. For example, using a very similar problem from location theory called the *attraction-repulsion problem* as a benchmark (a detailed review can be found in [39]), existing d.c. algorithms (e.g., [40], [64]) can require over 9 hours of computation time to generate $n = 1,000$ support points in $p = 2$ dimensions. To contrast, `sp.sbcd` requires only 30 seconds under the same setting! For higher-dimensional settings of $p > 2$ (which are of more practical interest), the proposed algorithms are much more practical than existing d.c. methods. Second, it is not clear how to incorporate a similar resampling scheme for F within d.c. methods (say, in the branch-and-bound algorithm in [40]) to achieve global convergence of $E(F, F_n)$. Despite these hurdles, the use of d.c. programming for global optimization is very tantalizing, and we will pursue this exciting algorithmic development in a future paper.

Regarding theory, there is still much work to be done to fully develop the proposed methodology. In particular, the simulations in Section 4 suggest the existence rate in Theorem 4 may be far from tight, and it would be of great value to explore a tighter rate which reflects the empirical performance of support points. Moreover, given its empirical improvement over IT-RSS for both small and moderate p , it is also worthwhile to explore whether support points enjoy a similar relief from dimensionality as MC and RQMC. Lastly, motivated by [27] and [28], integration points in high-dimensions should not only provide a good representation of F on the full space \mathcal{X} , but also for *marginal* distributions of F on *projected subspaces* of \mathcal{X} . New methodology is

therefore needed to incorporate the notion of *projected goodness-of-fit* within the support points framework.

Acknowledgments. This research is supported by the U. S. Army Research Office under grant number W911NF-14-1-0024.

APPENDIX A: ADDITIONAL PROOFS

A.1. Lemma 1. This proof is a straight-forward extension of Theorem 9.5.2 in [50], but we provide the full argument for clarity. Assume for brevity the univariate setting of $p = 1$, since the proof extends analogously for $p > 1$. Let $\Omega \subseteq \mathbb{C}$ be the set on which $\lim_{n \rightarrow \infty} \phi_n(t) = \phi(t)$. By the a.e. assumption, it follows that $\mu\{\Omega^c\} = 0$, where μ is the Lebesgue measure. We will first show that $\{F_n\}_{n=1}^\infty$ is *tight*, i.e., for all $\epsilon > 0$, \exists a finite interval $I \subset \mathbb{R}$ satisfying:

$$(27) \quad G(I^c) \leq \epsilon, \quad \forall F \in \{F_n\}.$$

To prove (27), fix $M > 0$, $\epsilon > 0$, and let $I = [-M, M]$. By Lemma 9.6.3 in [50], $\exists \alpha \in (0, \infty)$ satisfying:

$$\begin{aligned} \limsup_{n \rightarrow \infty} F_n(I^c) &\leq \limsup_{n \rightarrow \infty} \alpha M \int_{[0, M^{-1}]} \{1 - \operatorname{Re} \phi_n(t)\} dt \\ &= \limsup_{n \rightarrow \infty} \alpha M \left[\int_{[0, M^{-1}] \cap \Omega} \{1 - \operatorname{Re} \phi_n(t)\} dt + \int_{[0, M^{-1}] \cap \Omega^c} \{1 - \operatorname{Re} \phi_n(t)\} dt \right] \\ &= \limsup_{n \rightarrow \infty} \alpha M \int_{[0, M^{-1}] \cap \Omega} \{1 - \operatorname{Re} \phi_n(t)\} dt \\ &\quad \text{since } \mu\{[0, M^{-1}] \cap \Omega^c\} = 0, \\ &= \alpha M \int_{[0, M^{-1}] \cap \Omega} \limsup_{n \rightarrow \infty} \{1 - \operatorname{Re} \phi_n(t)\} dt \\ &\quad \text{by dominated convergence, since } 1 - \phi_n(t) \text{ is bounded,} \\ &= \alpha M \int_{[0, M^{-1}] \cap \Omega} \{1 - \operatorname{Re} \phi(t)\} dt. \end{aligned}$$

Since ϕ is a characteristic function, it follows that $\lim_{t \rightarrow 0} \phi(t) = 1$, so $\lim_{t \rightarrow 0} \{1 - \operatorname{Re} \phi(t)\} = 0$. Hence, for M sufficiently large, the above becomes:

$$\alpha M \int_{[0, M^{-1}] \cap \Omega} \{1 - \operatorname{Re} \phi(t)\} dt \leq \alpha M \int_{[0, M^{-1}] \cap \Omega} \epsilon dt = \alpha \epsilon,$$

which proves the tightness of $\{F_n\}$.

The remainder of the proof follows exactly as in Theorem 9.5.2 of [50]: one can show that any two convergent subsequences of $\{F_n\}$ must converge to the same limit, thereby proving the convergence of F_n to F . Readers can consult the aforementioned reference for details.

APPENDIX B: PLOTS OF SUPPORT POINTS

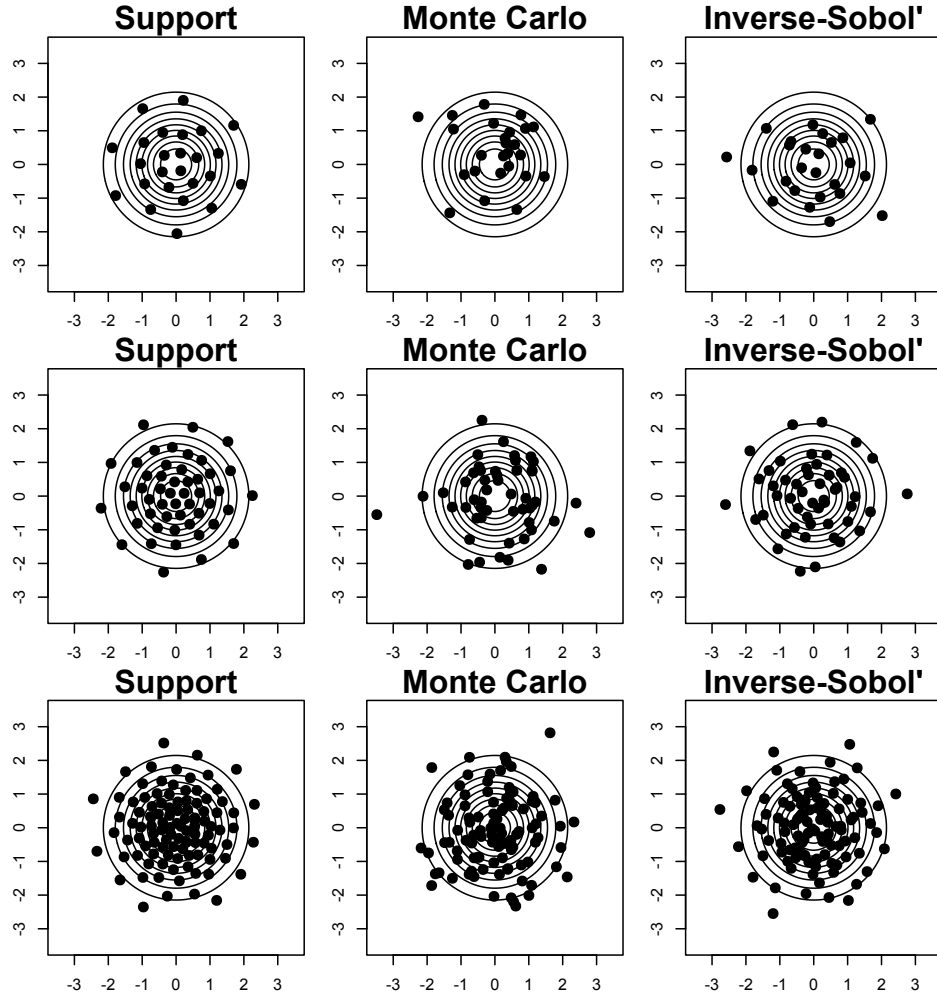


Figure 8: Plots of the $n = 25, 50$ and 100 support, MC and IT-RSS points for the i.i.d. $N(0, 1)$ distribution in $p = 2$ dimensions.

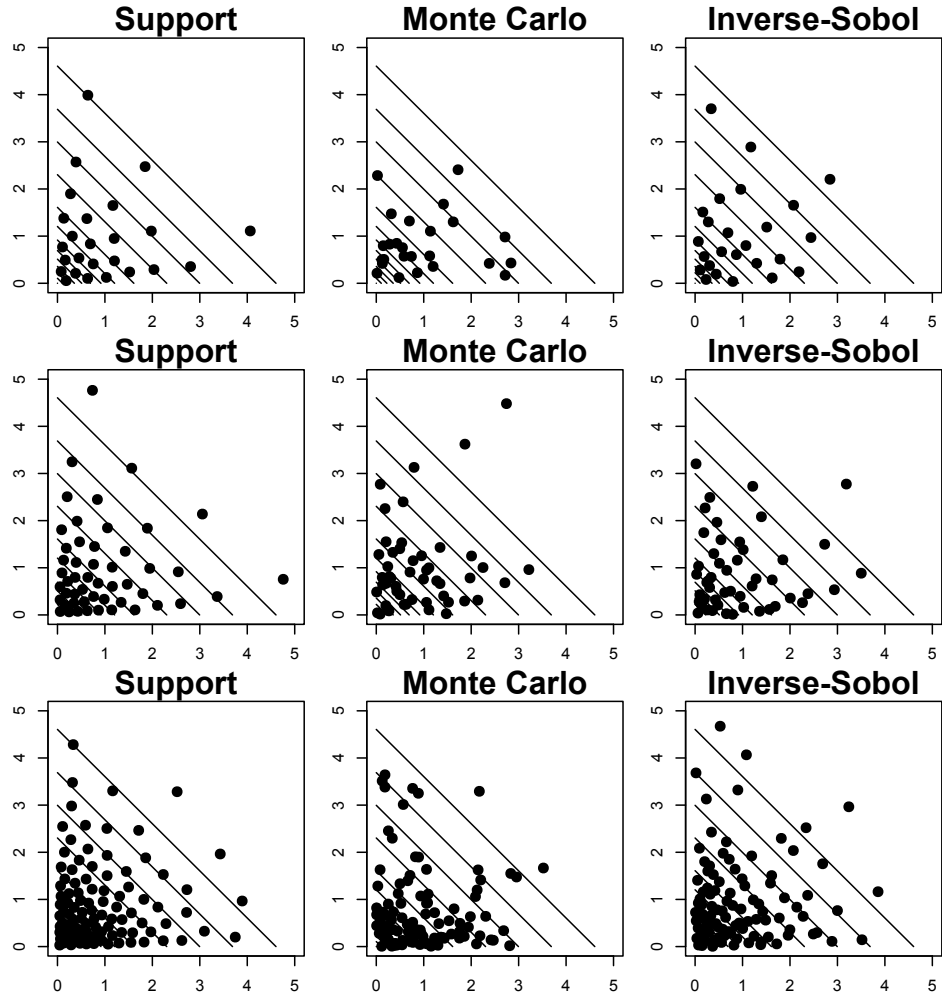


Figure 9: Plots of the $n = 25, 50$ and 100 support, MC and IT-RSS points for the i.i.d. $\text{Exp}(1)$ distribution in $p = 2$ dimensions.

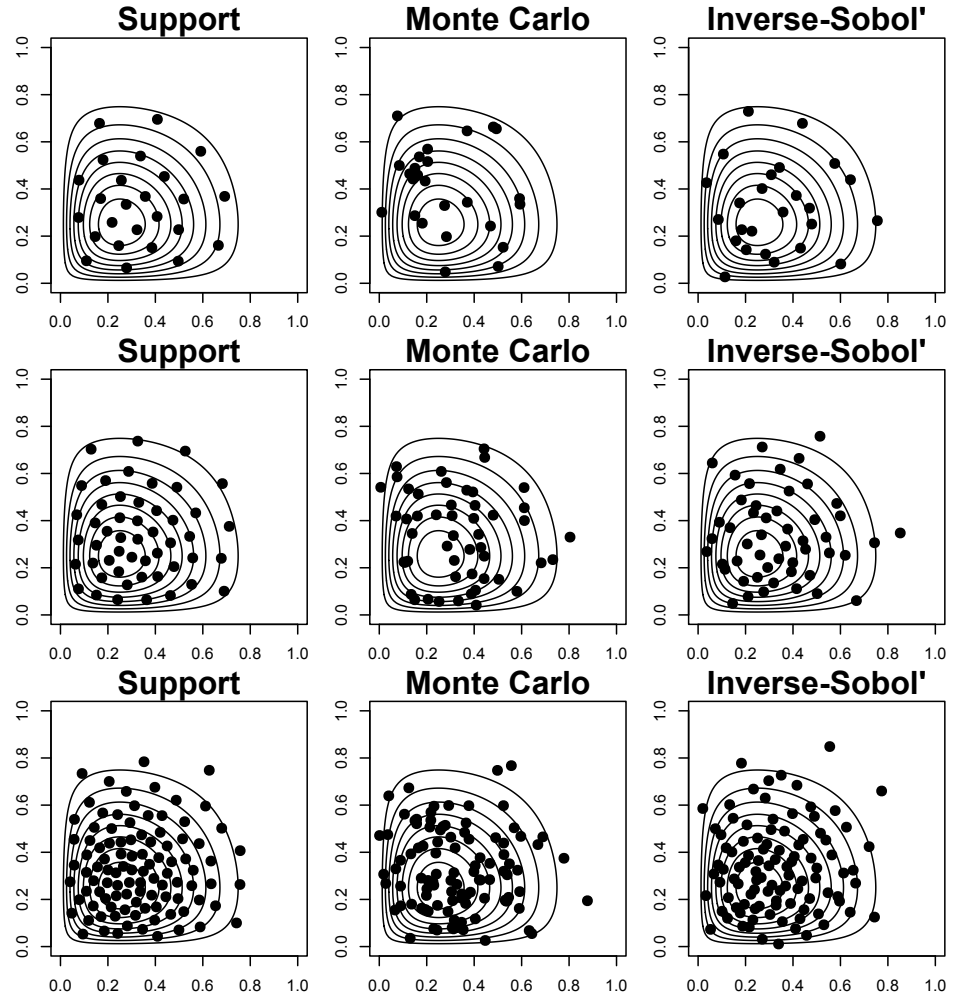


Figure 10: Plots of the $n = 25, 50$ and 100 support, MC and IT-RSS points for the i.i.d. $\text{Beta}(2, 4)$ distribution in $p = 2$ dimensions.

APPENDIX C: PLOTS OF INTEGRATION ERROR

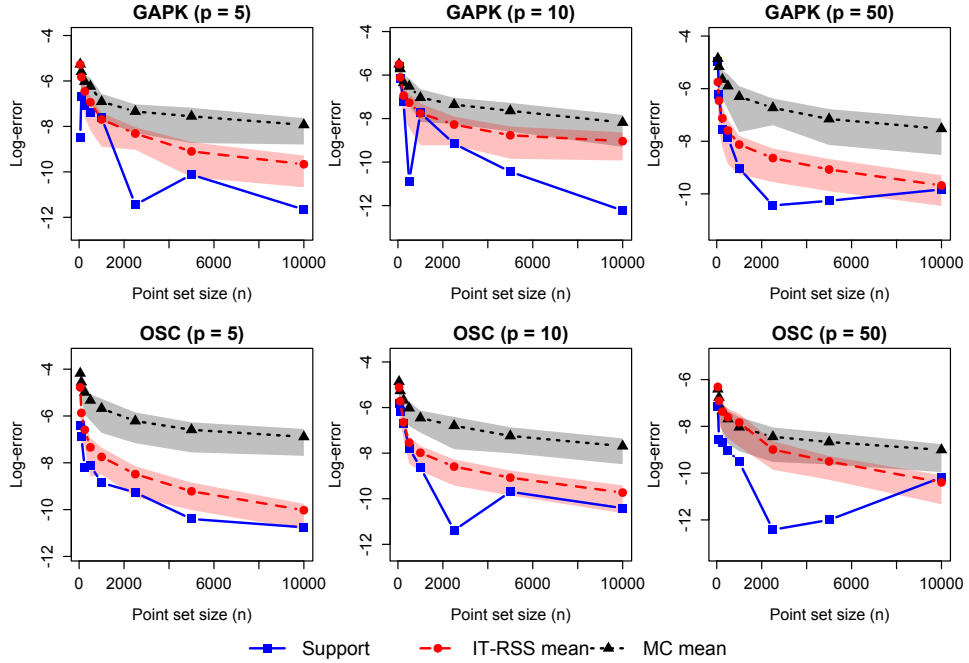


Figure 11: Log-absolute integration errors for the i.i.d. $N(0, 1)$ distribution in $p = 5, 10$ and 50 dimensions. Shaded regions indicate the 25-th and 75-th quantiles for MC and IT-RSS.

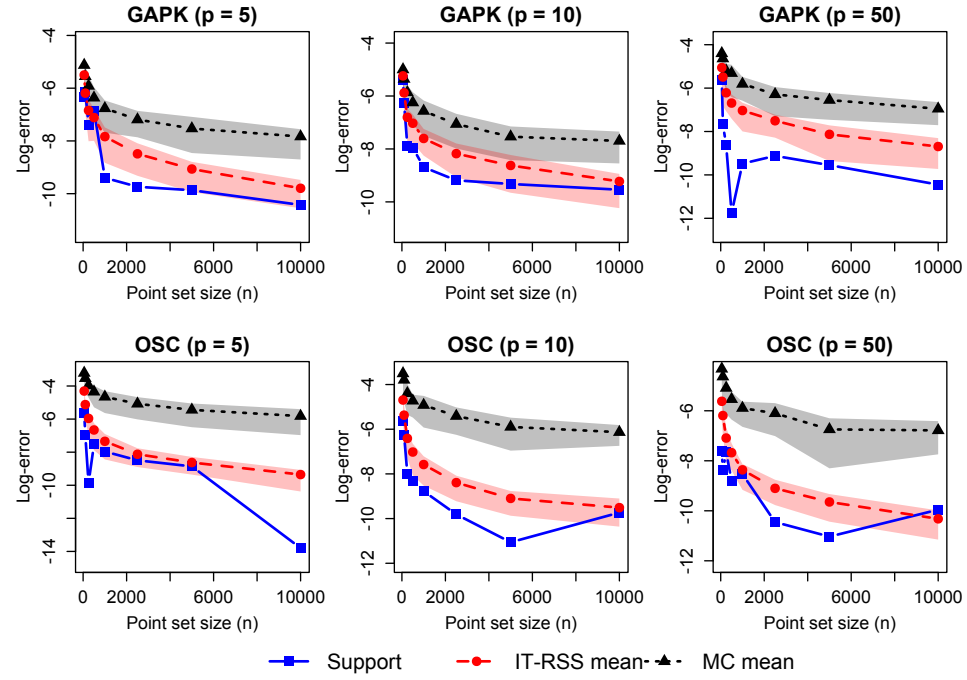


Figure 12: Log-absolute integration errors for the i.i.d. $\text{Exp}(1)$ distribution in $p = 5, 10$ and 50 dimensions. Shaded regions indicate the 25-th and 75-th quantiles for MC and IT-RSS.

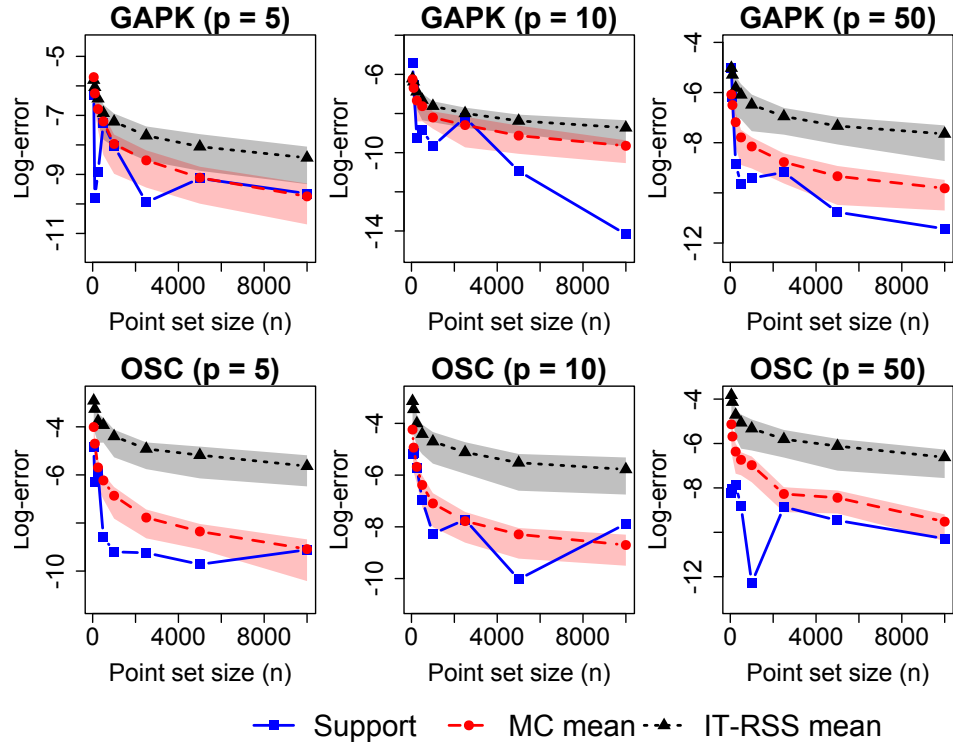


Figure 13: Log-absolute integration errors for the i.i.d. $\text{Beta}(2, 4)$ distribution in $p = 5, 10$ and 50 dimensions. Shaded regions indicate the 25-th and 75-th quantiles for MC and IT-RSS.

APPENDIX D: ROBOT ARM EMULATION EXAMPLE

The second example considers the emulation of a computer experiment model, which simulates the position of a robot arm with four segments (see 1 for details). This robot arm function, which we denote as h , takes in the following two inputs for each arm segment (8 inputs in total): $\theta_i \in [0, 2\pi]$, the angle of segment i , and $L_i \in [0, 1]$, the length of segment i . Letting $\mathbf{z} = (\theta_1, \dots, \theta_4, L_1, \dots, L_4)$, the explicit form of h is:

$$h(\mathbf{z}) = (u(\mathbf{x})^2 + v(\mathbf{z})^2)^{0.5}, \quad \text{where: } u = \sum_{i=1}^4 L_i \cos \left(\sum_{j=1}^i \theta_j \right), \quad v = \sum_{i=1}^4 L_i \sin \left(\sum_{j=1}^i \theta_j \right).$$

Suppose an experimenter does not know the explicit expression for h above, and the only way he or she can observe h is by plugging in an input \mathbf{z} into an expensive black-box simulator which outputs $h(\mathbf{z})$. Using a database of simulated inputs $\{\mathbf{z}_i\}_{i=1}^{n'}$ with corresponding outputs $\{h(\mathbf{z}_i)\}_{i=1}^{n'}$, the goal is to build a meta-model which predicts the unknown function h over its domain. For simplicity, we rescaled the original domain $[0, 2\pi]^4 \times [0, 1]^4$ to the unit hypercube $[0, 1]^8$.

We adopt a commonly-used method called *ordinary kriging* [52] to construct this meta-model. Ordinary kriging first models the unknown function h as a realization of the Gaussian process (GP):

$$(28) \quad Y(\mathbf{z}) = \eta + Z(\mathbf{z}), \quad \mathbf{z} \in [0, 1]^8.$$

Here, η is a constant mean parameter, and $Z(\mathbf{z})$ is a zero-mean GP with covariance function $\sigma^2 r(\cdot, \cdot)$. In this example, the following *Gaussian correlation* function is adopted for $r(\cdot, \cdot)$:

$$r(\mathbf{z}, \tilde{\mathbf{z}}) = \exp \left\{ - \sum_{l=1}^8 \theta_l (z^l - \tilde{z}^l)^2 \right\}.$$

Under this choice of correlation function, it can be shown that sample functions drawn from the GP (28) are infinitely differentiable [52]. For numerical stability, the correlation parameters $\theta_l \in [0, \infty)$ are reparameterized using the derived parameters $\rho_l \in [0, 1)$ through the transformation $\rho_l = \exp\{-\theta_l/4\}$.

Assume for now that the model parameters $\Theta = (\eta, \sigma^2, \rho_1, \dots, \rho_8)$ are known. Conditional on the vector of simulated outputs $\mathbf{h} = [h(\mathbf{z}_i)]_{i=1}^{n'}$, the MSE-optimal predictor of h at an unobserved input \mathbf{z}_{new} is:

$$(29) \quad \hat{h}(\mathbf{z}_{new}) = \mathbb{E}[h(\mathbf{z}_{new})|\mathbf{h}] = \eta + \mathbf{r}_{new}^T \mathbf{R}^{-1} (\mathbf{h} - \eta),$$

where $\mathbf{R} = [r(\mathbf{z}_i, \mathbf{z}_j)]_{i=1}^{n'}_{j=1}^{n'}$ is the $n' \times n'$ correlation matrix of simulated inputs, and $\mathbf{r}_{new} = [r(\mathbf{z}_{new}, \mathbf{z}_i)]_{i=1}^{n'}$ is the correlation vector for the new input \mathbf{z}_{new} . To foreshadow, we will introduce priors on the unknown parameters Θ , then compare how well support points and thinning estimate the posterior predictor $\mathbb{E}_{\Theta|\mathbf{h}}[\hat{h}(\mathbf{z}_{new})]$.

| Parameter | Distribution | $R(\mu, 375)$ | $R(\mu, 750)$ | $R(s, 375)$ | $R(s, 750)$ |
|--|--|---------------|---------------|-------------|-------------|
| η | $\eta \propto 1$ | 1.94 | 4.04 | 3.57 | 26.40 |
| σ^2 | $\sigma^2 \sim \text{Inv-Gamma}(0.1, 0.1)$ | 0.90 | 1.23 | 0.91 | 1.10 |
| ρ | $\rho_j \stackrel{i.i.d.}{\sim} \text{Beta}(1, 0.1)$ | 1.51 | 2.12 | 40.58 | 4.26 |
| $\mathbb{E}_{\Theta h}[\hat{h}(\mathbf{z}_{new}^{(1)})]$ | - | 5.94 | 7.46 | - | - |
| $\mathbb{E}_{\Theta h}[\hat{h}(\mathbf{z}_{new}^{(2)})]$ | - | 2.06 | 2.46 | - | - |
| $\mathbb{E}_{\Theta h}[\hat{h}(\mathbf{z}_{new}^{(3)})]$ | - | 5.27 | 9.05 | - | - |

Table 3: Prior specification for the robot arm model (left), and ratio of thinning over support-point error for posterior quantities (right). $R(\mu, n)$ and $R(s, n)$ denote the error ratio for posterior means and variances using n points, respectively.

As for the *design* of this emulator (i.e., the choice of points $\mathbf{z}_1, \dots, \mathbf{z}_{n'}$ at which the simulation is run), we use the standard maximin Latin hypercube design [41], although more elaborate schemes such as the MaxPro designs [28] or miniMaxPro designs [38] may be of interest for further studies.

The problem is that the GP model parameters Θ are unknown in practice, and thus require estimation using simulation data. Similar to the first example, we adopt a Bayesian approach and perform MCMC sampling on the posterior distribution of Θ . The following prior specification is imposed:

$$\eta \propto 1, \sigma^2 \sim \text{Inv-Gamma}(0.1, 0.1), \rho_1, \dots, \rho_8 \stackrel{i.i.d.}{\sim} \text{Beta}(1, 0.1).$$

As in the first example, STAN is used to conduct MCMC sampling of the posterior, with the chain run for 60,000 iterations and the first 30,000 of these discarded as burn-in. The remaining $N = 30,000$ posterior samples are then thinned by a rate of 100 and 50, giving $n = 300$ and 600 samples respectively, and support points are computed for the same choices of n . The true value of the prediction $\mathbb{E}_{\Theta|h}[\hat{h}(\mathbf{z}_{new})]$ is again approximated by running a longer MCMC chain with 180,000 iterations, 90,000 of which are burn-in.

Table 3 summarizes the ratio of absolute errors using support points and thinning for the marginal means and standard deviations of each parameter, along with the emulator predictors $\mathbb{E}_{\Theta|h}[\hat{h}(\mathbf{z}_{new})]$ for three choices of \mathbf{z}_{new} : $\mathbf{z}_{new}^{(1)} = 0.5 \cdot \mathbf{1}_8$, $\mathbf{z}_{new}^{(2)} = (0.6 \cdot \mathbf{1}_4, 0.4 \cdot \mathbf{1}_4)$ and $\mathbf{z}_{new}^{(3)} = \mathbf{1}_4 \otimes (0.6, 0.4)$. Again, for brevity, we report only the average ratio of absolute errors for the 8 correlation parameters ρ_1, \dots, ρ_8 . The same two observations from the first example also hold here. First, error ratios are greater than 1 for nearly all posterior quantities, which affirms the superiority of support points over thinning. Second, nearly all of these ratios increase as the thinning rate decreases, which confirms the faster convergence rate enjoyed by support points.

REFERENCES

- [1] An, J. and Owen, A. (2001). Quasi-regression. *Journal of complexity*, 17(4):588–607.
- [2] Auslender, A. (1976). *Optimisation: Méthodes Numériques*. Masson.
- [3] Borodachov, S. V., Hardin, D. P., and Saff, E. B. (2014). Low complexity methods for discretizing manifolds via Riesz energy minimization. *Foundations of Computational Mathematics*, 14(6):1173–1208.
- [4] Chelson, P. O. (1976). *Quasi-random techniques for Monte Carlo methods*. Claremont Graduate School.
- [5] Chen, S., Dick, J., and Owen, A. B. (2011). Consistency of Markov chain quasi-Monte Carlo on continuous state spaces. *The Annals of Statistics*, 39(2):673–701.
- [6] Chen, X. (2012). Smoothing methods for nonsmooth, nonconvex minimization. *Mathematical Programming*, 134(1):71–99.
- [7] Chentsov, N. (1967). Pseudorandom numbers for modelling Markov chains. *USSR Computational Mathematics and Mathematical Physics*, 7(3):218–233.
- [8] Cobos, F. and Kühn, T. (1990). Eigenvalues of integral operators with positive definite kernels satisfying integrated Hölder conditions over metric compacta. *Journal of Approximation Theory*, 63(1):39–55.
- [9] Cox, D. R. (1957). Note on grouping. *Journal of the American Statistical Association*, 52(280):543–547.
- [10] Dalenius, T. (1950). The problem of optimum stratification. *Scandinavian Actuarial Journal*, 1950(3-4):203–213.
- [11] Dasgupta, R. (2015). *Growth Curve and Structural Equation Modeling*. Springer.
- [12] Dick, J., Kuo, F. Y., and Sloan, I. H. (2013). High-dimensional integration: the quasi-Monte Carlo way. *Acta Numerica*, 22:133–288.
- [13] Dick, J. and Pillichshammer, F. (2010). *Digital nets and sequences: Discrepancy Theory and Quasi-Monte Carlo Integration*. Cambridge University Press.
- [14] Doob, J. L. (2012). *Classical Potential Theory and Its Probabilistic Counterpart: Advanced Problems*, volume 262. Springer Science & Business Media.
- [15] Draper, N. R. and Smith, H. (1981). *Applied Regression Analysis*. John Wiley & Sons.
- [16] Dutang, C. and Savicky, P. (2013). randtoolbox: Generating and testing random numbers. *R package*, page 67.
- [17] Fang, K.-T. (1980). The uniform design: Application of number-theoretic methods in experimental design. *Acta Math. Appl. Sinica*, 3(4):363–372.
- [18] Fang, K.-T., Lu, X., Tang, Y., and Yin, J. (2004). Constructions of uniform designs by using resolvable packings and coverings. *Discrete Mathematics*, 274(1):25–40.
- [19] Fang, K.-T. and Wang, Y. (1994). *Number-theoretic Methods in Statistics*, volume 51. CRC Press.
- [20] Flury, B. A. (1990). Principal points. *Biometrika*, 77(1):33–41.
- [21] Friedman, J., Hastie, T., and Tibshirani, R. (2008). Sparse inverse covariance estimation with the graphical lasso. *Biostatistics*, 9(3):432–441.
- [22] Friedman, J., Hastie, T., and Tibshirani, R. (2010). Regularization paths for generalized linear models via coordinate descent. *Journal of Statistical Software*, 33(1):1.
- [23] Genz, A. (1984). Testing multidimensional integration routines.
- [24] Geyer, C. J. (1992). Practical Markov chain Monte Carlo. *Statistical Science*, 7(4):473–483.
- [25] Graf, S. and Luschgy, H. (2000). *Foundations of quantization for probability distributions*. Springer-Verlag Berlin Heidelberg.
- [26] Gregory, G. G. (1977). Large sample theory for U-statistics and tests of fit. *The*

Annals of Statistics, pages 110–123.

[27] Hickernell, F. (1998). A generalized discrepancy and quadrature error bound. *Mathematics of Computation of the American Mathematical Society*, 67(221):299–322.

[28] Joseph, V. R., Dasgupta, T., Tuo, R., and Wu, C. F. J. (2015). Sequential exploration of complex surfaces using minimum energy designs. *Technometrics*, 57(1):64–74.

[29] Kiefer, J. (1961). On large deviations of the empiric df of vector chance variables and a law of the iterated logarithm. *Pacific Journal of Mathematics*, 11(2):649–660.

[30] Kolmogorov, A. N. (1933). *Sulla determinazione empirica di una legge di distribuzione*.

[31] Korolyuk, V. and Borovskikh, Y. V. (1984). Asymptotic analysis of distributions of statistics. *Naukova Dumka, Kiev*, page 304.

[32] Kuo, F. Y. and Sloan, I. H. (2005). Lifting the curse of dimensionality. *Notices of the AMS*, 52(11):1320–1328.

[33] Lange, K. (2010). *Numerical Analysis for Statisticians*. Springer Science & Business Media.

[34] Link, W. A. and Eaton, M. J. (2012). On thinning of chains in MCMC. *Methods in Ecology and Evolution*, 3(1):112–115.

[35] Lloyd, S. (1982). Least squares quantization in PCM. *Information Theory, IEEE Transactions on*, 28(2):129–137.

[36] Luenberger, D. G. and Ye, Y. (2008). *Linear and Nonlinear Programming*, volume 116. Springer Science & Business Media.

[37] Mairal, J. (2013). Stochastic majorization-minimization algorithms for large-scale optimization. In *Advances in Neural Information Processing Systems*, pages 2283–2291.

[38] Mak, S. and Joseph, V. R. (2016). Minimax designs using clustering. *arXiv preprint arXiv:1602.03938*.

[39] Maranas, C. D. (2008). Global optimization in Weber’s problem with attraction and repulsion. In *Encyclopedia of Optimization*, pages 1423–1427. Springer.

[40] Maranas, C. D. and Floudas, C. A. (1994). A global optimization method for Webers problem with attraction and repulsion. In *Large Scale Optimization*, pages 259–285. Springer.

[41] Morris, M. D. and Mitchell, T. J. (1995). Exploratory designs for computational experiments. *Journal of statistical planning and inference*, 43(3):381–402.

[42] Nichols, J. A. and Kuo, F. Y. (2014). Fast CBC construction of randomly shifted lattice rules achieving $\mathcal{O}(n^{-1+\delta})$ convergence for unbounded integrands over \mathbb{R}^s in weighted spaces with POD weights. *Journal of Complexity*, 30(4):444–468.

[43] Niederreiter, H. (2010). *Quasi-Monte Carlo Methods*. Wiley Online Library.

[44] Nuyens, D. and Cools, R. (2006). Fast algorithms for component-by-component construction of rank-1 lattice rules in shift-invariant reproducing kernel Hilbert spaces. *Mathematics of Computation*, 75(254):903–920.

[45] Ortega, J. M. and Rheinboldt, W. C. (1970). *Iterative solution of nonlinear equations in several variables*, volume 30. SIAM.

[46] Owen, A. B. (1998). Scrambling Sobol’ and Niederreiter–Xing points. *Journal of Complexity*, 14(4):466–489.

[47] Pagès, G., Pham, H., and Printems, J. (2004). Optimal quantization methods and applications to numerical problems in finance. In *Handbook of Computational and Numerical Methods in Finance*, pages 253–297. Springer.

[48] Paley, R. and Zygmund, A. (1930). On some series of functions. In *Mathematical Proceedings of the Cambridge Philosophical Society*, volume 26, pages 337–357. Cambridge Univ Press.

[49] Razaviyayn, M., Hong, M., and Luo, Z.-Q. (2013). A unified convergence analysis of block successive minimization methods for nonsmooth optimization. *SIAM Journal on*

Optimization, 23(2):1126–1153.

[50] Resnick, S. I. (1999). *A Probability Path*. Springer Science & Business Media.

[51] Rosenblatt, M. (1952). Remarks on a multivariate transformation. *The Annals of Mathematical Statistics*, pages 470–472.

[52] Santner, T. J., Williams, B. J., and Notz, W. I. (2013). *The Design and Analysis of Computer eExperiments*. Springer Science & Business Media.

[53] Sloan, I. H., Kuo, F. Y., and Joe, S. (2002). Constructing randomly shifted lattice rules in weighted Sobolev spaces. *SIAM Journal on Numerical Analysis*, 40(5):1650–1665.

[54] Sobol', I. M. (1967). On the distribution of points in a cube and the approximate evaluation of integrals. *Zhurnal Vychislitel'noi Matematiki i Matematicheskoi Fiziki*, 7(4):784–802.

[55] Stan Development Team (2015). Stan: A C++ library for probability and sampling, version 2.10.0.

[56] Su, Y. (2000). Asymptotically optimal representative points of bivariate random vectors. *Statistica Sinica*, 10(2):559–576.

[57] Székely, G. J. and Rizzo, M. L. (2004). Testing for equal distributions in high dimension. *InterStat*, 5:1–6.

[58] Székely, G. J. and Rizzo, M. L. (2005). A new test for multivariate normality. *Journal of Multivariate Analysis*, 93(1):58–80.

[59] Székely, G. J. and Rizzo, M. L. (2013). Energy statistics: A class of statistics based on distances. *Journal of Statistical Planning and Inference*, 143(8):1249–1272.

[60] Tao, P. D. and An, L. T. H. (1997). Convex analysis approach to dc programming: Theory, algorithms and applications. *Acta Mathematica Vietnamica*, 22(1):289–355.

[61] Tribble, S. D. (2007). *Markov chain Monte Carlo algorithms using completely uniformly distributed driving sequences*. PhD thesis, Stanford University.

[62] Tuo, R. and Lv, S. (2016). Limiting distributions of the minimum energy designs.

[63] Tuy, H. (1995). Dc optimization: theory, methods and algorithms. In *Handbook of Global Optimization*, pages 149–216. Springer.

[64] Tuy, H., Al-Khayyal, F., and Zhou, F. (1995). A dc optimization method for single facility location problems. *Journal of Global Optimization*, 7(2):209–227.

[65] Warnock, T. T. (1995). Computational investigations of low-discrepancy point sets ii. In *Monte Carlo and Quasi-Monte Carlo Methods in Scientific Computing*, pages 354–361. Springer.

[66] Worley, B. A. (1987). Deterministic uncertainty analysis.

[67] Yang, G. (2012). *The energy goodness-of-fit test for univariate stable distributions*. PhD thesis, Bowling Green State University.